Nanofluids for direct cooling application in a diesel engine

Master's thesis in Energy technology

Thermal Machines

Sturla Grina Ruud

University of Bergen,

Geophysical Institute

Western University of Applied Sciences,

Institute of Mechanical and Marine Engineering

Bergen, 31th of May 2023

Nanofluids for direct cooling application in a diesel engine

Sturla Grina Ruud

University of Bergen (UiB)
Faculty of Mathematics and Natural Sciences
Geophysical Institute
Post box 7803
5020 Bergen, Norway

In cooperation with:
Western University of Applied Sciences (HVL)
Faculty of Engineering and Science
Institute of Mechanical and Marine Engineering
Post box 7030
5020 Bergen, Norway

Norsk tittel:	**Direkte bruk av nanofluider som kjølevæske i en dieselmotor**
Author, student-ID:	**Sturla Grina Ruud** , 310652/602976
Study program:	Energy technology, Thermal machines
Date:	31.05.2023
Supervisor(s) at HVL:	Boris Balakin Pavel Struchalin Peter Edgard Koch
Supervisor(s) at UiB:	Pawel Kosinski
Thesis Coordinator:	HVL
Coordinators reference	Peter Edgard Koch
Number of digitaly submitted files:	1

Acknowledgements

This work is the work carried out over the 2023 spring semester and represents the final evaluation of a two-year master's program in Energy technology, with a specialization in thermal machines. I would like to direct my appreciation to the Western University of Applied Sciences (HVL) and the University of Bergen (UiB) as these past years have been enlightening and given me the right tools for writing my master's thesis.

The final product would not have been possible without the guidance I received from my terrific supervisors. I would therefore firstly like to thank Boris Balakin, Pavel Struchalin, Peter Koch, and Pawel Kosinski. Thank you for your excellent guidance, insightful comments, and interest in helping me create this work. Secondly, I would like to thank the engineers at the Department of Mechanical and Marine Engineering at HVL, Harald Moen, and Frode Wessel Jansen for their efforts in making sure I could perform my experiments with the engine. Your efforts were greatly appreciated. I would also like to extend a thank you to Yansong Zhang for his help in the chemistry lab and with additional viscosity measurements. Fourth, I would like to say thank you to all my family and friends who were kind enough to provide me with helpful feedback on various drafts throughout this process. Additionally, I would like to extend my appreciation to the ELMILAB at the University of Bergen for their help with the electron microscopy.

Sturla Grina Ruud
Bergen, 31.05.2023

Abstract

The work carried out in this thesis is the characterization and investigation of carbon-based nanofluids as a potential engine coolant for a single-cylinder diesel engine. Carbon black particles could be sufficiently stabilized with a 1:10 wt. ratio of PVP. Given a 1 hour sonication time. This was done for samples containing 0.5wt.%, 1wt.%, 2.5wt.%, 5wt.%, 7.5wt.% and 10wt.% nanoparticles. The physical properties of the different nanofluid samples were studied. This includes experimental testing for stability to static and thermal load. Which was quantified using Ultraviolet visible spectroscopy and particle size distribution. How particles and basefluid influences nanofluid viscosity was determined experimentally through viscosity measurements. Additionally, these data were further investigated using Brinkman's and Einstein's equations. Nanofluid's thermal conductivity was decided by testing common effective medium theories to previous measurement data and new measurement data using a transient hot wire. The nanofluid properties were used to evaluate what fluids should be used as coolants in the compression-ignited engine. It was found that there was little change when considering the general trend for static stability over two weeks. Thermal stability was however difficult to characterize, and the reason for this is not known. Additionally, thermophysical properties were used to determine the relative effectiveness of different samples of nanofluids compared to water, using so-called "figure of merit" equations. This showed that concentrations 2.5wt.% and 0.5wt.% carbon black had the best properties as an engine coolant. The heat transfer of these nanofluids was compared to the rate of heat transfer of water, and ethylene glycol in water at flow rates of 3, 4, and 5 liters per minute. No clear trend was found for the nanofluids, and at this time is thought to offer little benefit as an engine coolant. However, more work is needed on the subject.

Contents

List of Figures

List of Tables

Chapter 1

Introduction

As the industrial revolution started to take place in the final half of the 18th century, human civilization was entering a new chapter that would fundamentally change the way of living. One of the reasons that allowed for such a transformation to take place was the development of new technologies, such as the use of coal and the steam engine, the rafining of petroleum, electricity, and the internal combustion engine (ICE) [5]. There is no doubt that thermal energy has been a key element to humanity's success. As thermal energy has been the dominant energy form that ensures power generation, heating, and transportation in the world. One of the critical aspects of thermal machinery is cooling, which allows for the transport of thermal energy from high temperatures to lower temperatures.

Ever since the first thermal machines continuous development has been made for making more efficient cooling systems, which have higher and higher rates of heat transfer [6]. Water has been used in a lot of heat transfer processes as the working fluid. However, the thermal conductivity of fluids such as water is low compared to other materials, like copper [1]. The low thermal conductivity has been a restricting factor for further development in heat transfer. This problem is exactly what led researchers at the Argonne National Laboratory to the development of a new type of fluid. *Nanofluid* is a term coined by Choi and Eastman in 1995 [7], which found that adding copper *nanoparticles* in water increased the thermal conductivity. The first recorded example of increased thermal conductivity by nanoparticle suspension was however done by Masuda *et al.* in 1993 [8].

Nanofluids are colloids of nanoparticles, with a diameter usually less than 100 nm in a basefluid, such as water or ethylene glycol. These colloids can exhibit unique thermal, electrical, and optical properties that are not found in the basefluid alone [2]. These fluids have the potential to improve the performance of various industrial and technological applications [9]. One of these areas is the cooling of internal combustion engines. Even though organizations such as the EU are enforcing stricter emissions for combustion engines used in vehicles [10]. New and exciting research is begin conducted for alternative types of fuel, and fuel systems [11, 12, 13]. Additionally, there are several issues associated with phasing out ICE vehicles too soon [14].

So why focus research on nanofluids for the application of engine cooling? Nanofluid

research is widely applicable [15] within thermal systems, as the governing principles of heat transfer do not change. Making more efficient cooling systems will in the future allow for making them more compact. The potential size reduction of cooling systems can allow for better design. One example of this is how a redesigned nanofluid radiator could allow for reduced drag on a vehicle, increasing fuel efficiency and decreasing emissions [16]. However, the potential in reducing required space could offer huge advantages for other engine systems, such as in shipping or power generation.

1.1 Problem Statement and objectives

This thesis represents the work carried out over the course of a semester and will experimentally investigate the potential for increased heat transfer using nanofluids as a coolant in a single-cylinder diesel engine.

Nanofluids offer potential huge upsides with regard to cooling applications. The goal of this work is to generate information on the use of carbon black in cooling systems to determine its effectiveness in engine cooling. In order to do this, the following problem statement has been formulated:

> *Does carbon black-based nanofluids offer any benefits for cooling the engine head in a one-cylinder 6kW compression-ignited diesel engine, compared to other coolants?*

In order to accurately answer the problem statement, a list of relevant objectives has been formulated in order to accumulate the necessary information in order to draw a conclusion. The objectives of this work are to:

1. Find a suitable nanofluid composition.
2. Acquire and characterize nanofluid properties.
3. Investigate optimal nanoparticle concentration.
4. Perform testing with nanofluid as engine coolant.
   (a) Perform testing with particle free coolant.
   (b) Compare heat transfer from nanofluid with heat transfer from the particle free coolant.

Chapter 2

Theory

This chapter will present an introduction to relevant theory and literature, which is essential to the core subjects of this work. These subjects are fluid behavior, heat transfer, nanofluids, and engine cooling.

2.1 Fluid dynamic principles

2.1.1 Fluid viscosity

Viscosity refers to two types of qualities. Dynamic and kinematic viscosity. Kinematic viscosity is defined as the ratio of dynamic viscosity to the density of the fluid. Dynamic viscosity μ, in a fluid is the ratio of shear stress over the velocity gradient. A fluid with lower viscosity will flow and respond quickly to changes in its environment. On the contrary, a viscous fluid will flow slower under the same conditions. It is therefore commonly formulated that viscosity is a measurement of the resistance of a fluid to deformation, or flow [1]. A fluid's viscosity can be affected by two types of stress. *Shear stress* and *normal stress*. Normal stress could occur parallel and perpendicular to fluid flow. This manifests either as flow pressure (parallel) or compression (perpendicular). Shear stress happens when the fluid's parallel "layers" (these layers are described in section 2.1.2) during flow [17]. However, not all fluids respond equally to shear stress. A linear increase in shear stress with shear rate would classify a Newtonian fluid, whereas a non-linear increase would indicate a non-Newtonian fluid. There are different classifications for how fluid flow is affected by shear stress τ and time [1]. Table 2.1 gives an overview of some typical rheological classifications of fluids [1].

Table 2.1: Rhelogical classifications of fluids from [1]

Classification	Dependence on increasing shear rate	Time dependence	Example
Pseudoplastic	Thins	No	Polymer solutions
Thixotropic	Thins	Yes	Some polymer solutions
Newtonian	None	No	Most simple liquids, e.g. water
Dilatant	Thickens	No	Starch in water

As stated by table 2.1, most simple liquids are Newtonian, this includes water. The proportionality constant between shear stress and shear rate is the viscosity. This can be

defined by newtons law of friction for one direction as in equation (2.1) for Newtonian fluids as one-dimensional flow [1].

$$\tau = \mu \frac{dv_x}{dy} \tag{2.1}$$

Where $\tau = \frac{F}{A}$ is the shear stress (force over area) and the velocity gradient in x direction, of the fluid is defined by $\frac{dv_x}{dy}$, away from some boundary in the y direction [1]. On the molecular level, viscosity occurs due to the internal interaction of the fluid molecules. More interaction means more friction and more resistance to flow [17]. The temperature will therefore affect viscosity. As the fluid molecules gain energy, the contact between them will vary, altering the intermolecular forces. This can result in both increase and decrease in viscosity depending on the medium. However, the viscosity will decrease with temperature in most liquids. Viscous fluids traveling at high velocities may also generate heat due to friction of the surrounding walls [1].

Viscosity is an important parameter for heat exchange systems. Convective heat transfer and pressure drop will influence the friction generated, which must be accounted for by increased pump work. Over the years several theoretical methods have been developed to estimate the viscosity of colloids and suspensions. In 1905 Einstein developed a formula for calculating the viscosity of a fluid containing spherical particles at low volume fractions that there are no particle-to-particle interactions [18]. Einstein suggested that adding small spherical particles would increase the internal friction due to particle-liquid interactions [19].

$$\mu_{\text{nf}} = \mu_{\text{bf}} \times (1 + 2.5\varphi) \tag{2.2}$$

The viscosity of the nanofluid is given by μ_{nf}. Whereas μ_{bf} denotes the viscosity of the basefluid. The volumetric fraction of particle suspension is given by φ. The formula describes that there will be a linear increase in the viscosity of the nanofluids, as the particle concentration increases. The formula has some limitations, as it does not take into account agglomerate structure, particle-to-particle interaction, and high particle concentration [20]. Einstein's equation is therefore restricted to $\varphi \leq 0.02$ [21].

Brinkman expanded on Einstein's work in 1952 [22]. Brinkman's equation considers the effect of adding particles to an existing solution of particles. The formula accounts for particle concentrations less than $\varphi \leq 0.04$ [20]. The equation is given in (2.3).

$$\frac{\mu_{\text{nf}}}{\mu_{\text{bf}}} = (1 - \varphi)^{-2.5} \tag{2.3}$$

However, regarding suspensions several experiments show that there are many factors that can influence such fluid's viscosity. This includes particle size and shape, concentration, temperature, dispersants, and pH levels [20]

2.1.2 Fluid flow

A fluid flow is often categorized into two different types of flow regimes. As the fluid flows at low velocity, it tends to flow without self-mixing and stirring. This type of behavior is characterized as laminar flow and is characterized as being made up of many

smooth flowing layers [1].

As the velocity of the fluid increases past what is called *critical flow*, the flow becomes more and more erratic and unpredictable. As this happens, the fluid self-mixes and stirs due to the creation of cross-currents and eddies [1]. Eddies have a defined amount of mechanical energy which is supplied by the bulk flow of the fluid. Larger eddies will break down transferring their energy into smaller and smaller eddies. The smallest eddies are in the range of 10-100μm. Which is about 10^{12} molecules. After this point, the remaining energy dissipates into heat. This type of fluid flow is called turbulent flow [1]. Turbulent flow was studied by Reynolds, who concluded that at the critical velocity, where laminar flow changes to turbulent are dependent on pipe diameter d viscosity μ, density ρ and average fluid velocity $\bar{v}$. The formulation of the dimensionless Reynolds number is given in equation (2.4) [1].

$$Re = \frac{D\bar{v}\rho}{\mu} \tag{2.4}$$

Typically, a Reynolds number below 2100 for water in a smooth pipe would be characterized as laminar. However, surface roughness, type of liquid, and flow geometry will greatly influence at what intervals Reynolds number equates to laminar and turbulent. Particularly flow past immersed objects will influence turbulence [1].

As fluid flows along some boundary like a surface, the fluid molecules will experience a greater resistance to motion the closer to the surface they are. The fluid molecules furthest away have no interaction with the surface. Meaning that fluid velocity will decrease the closer it is to a surface. The result of this is the creation of a layer of laminar flowing fluid that will form near the boundary, whereas further away the flow can be turbulent. This layer is called the hydrodynamic boundary layer. At the surface, the fluid velocity is nonexistent, also known as the no-slip condition. The region between these two states of laminar (viscus sublayer) and turbulent boundary layer is named the buffer layer [1]. When fluid flows in a tube, the hydrodynamic boundary layer increases in thickness, as it moves along the tube away from the inlet. Much like what is shown by line **OA** in figure 2.1. When the boundary layer reaches the center of the tube, the velocity profile reaches what is called *fully developed flow*, which will not change with additional length [1].

2.2 Heat and mechanisms of transfer

2.2.1 An introduction to heat

Heat Q, is a concept that can be described by the terms *thermal energy* and *internal energy* [23]. The thermal energy of some substance can be thought of as the sum of all the energy, through random movement, rotation, and vibration in a number of microscopic particles that make up a larger macroscopic system. Examples of such systems would be a gas or a liquid [23].

The system's temperature T is a relative measurement for the system's energy levels as a whole. When thermal energy is transferred to a system of particles (like a gas). The molecules that make up that gas will have their kinetic energy increased. Making the macroscopic energy levels of the system, or temperature rise [23].

The internal energy U, is the total sum of all the energy in an isolated system or subsystem. The system's kinetic or potential energy is therefore not considered [23]. In a thermodynamic process, the internal energy is a function of the system's temperature. The definition of internal energy is presented in equation (2.5). Where the dT is the infinitesimal change of temperature, and C_V is the specific heat capacity under constant volume [24].

$$\Delta U = U_2 - U_1 = \int_1^2 C_V dT \tag{2.5}$$

The change or transfer of thermal energy is defined as heat. Consider a body at absolute zero of temperature 0K or -273.15°C . This body will have no thermal energy, making all particles stay fixed [23]. If this body is exposed to a substance with another temperature, thermal energy will transfer due to the difference in temperature [25]. This happens until both the body and the substance is at the same temperature or thermal equilibrium. This is known as the 0^{th} law of thermodynamics [24]. As the temperature of the body goes up, the internal energy will increase. This process is described as heating. Making heat the transfer of thermal energy, which occurs because of the difference in the temperature.

2.2.2 Mechanisms of heat transfer

Heat transfer can occur in three main ways. These are known as *conduction*, *convection*, and *radiation* [24]. Conduction is the transfer of energy over a temperature difference. Energy internally in the system is transferred from particle to particle due to internal collisions. The macroscopic result of this is the transfer of heat. The change of heat in a material can be described by the heat equation (2.6) which is a special case of the diffusivity equation. In which the conductivity throughout a body in three dimensions, the thermal conductivity coefficient is denoted by k. The negative sign denotes that heat goes from warmer to colder. The specific heat capacity of the material is denoted by C_p and ρ is the density of the fluid. The heat rate is described by the left-hand side of the equation [26]. The right-hand side of the equation shows how the rate of heat is dependent on the change in temperature through the material.

$$C_p \rho \frac{\partial T}{\partial t} = \nabla \cdot (-k \nabla T) \tag{2.6}$$

Often, several simplifications are made. If the material through which heat conducts is the same in all directions (isotropic), the heat capacity, density, and thermal conductivity coefficient are constants. Another simplification would be that the change in temperature is constant.

Convection is a phenomenon that includes a flowing medium. It can be thought of as the transportation of heat in a fluid and is dependent on the movement of the fluid. Convection can take place in two forms. This is as natural and forced convection. Heat transfer through convection is also dependent on a temperature difference, the same way conduction does. The rate of heat transfer is dependent on a heat transfer coefficient, the same way the rate of conduction is dependent on k.

When considering a laminar flowing fluid at either constant temperature or with a constant heat flux along the fluid boundary, the temperature gradient will reach a certain point where the viscosity will change along the fluid flow over the boundary. This can cause the velocity distribution of the fluid to change. As the change happens, the fluid closes to the boundary can have a different viscosity than the fluid furthest away from the boundary. The result of this occurrence is internal cross-flows as the velocity closer to the boundary increases. Furthermore, temperature differences will cause a density gradient in the fluid which will be driving the internal transportation of the fluid across ”layers”. This happens because the fluid with the lower density will rise above the higher density. When either one or both of these phenomena occurs, there is said to be natural convection [1].

Forced convection is the transport of fluid, in which an external force is generating the movement and internal transport in the fluid. An example of this is the use of a pump to push the fluid through some system. In forced convection systems, some natural convection will be present [1].

radiation can be described as the admittance of energy from the electromagnetic spectrum. A simple model for radiation is black body radiation. Which means a body that will absorb and emit all electromagnetic waves [1].

$$\frac{Q}{A} = \sigma\varepsilon({T^4}_2 - {T^4}_1) \tag{2.7}$$

I which σ is used to represent the Boltzmann constant $\sigma = 5.6 \cdot 10^{-8}\mathrm{W/m^2K^4}$, ε is the emissivity and varies between 0 and 1, and T is the temperature in Kelvin [1].

2.2.3 Thermal boundary layer

Consider a steady flow fluid with a temperature T_∞, a velocity $v = 0$ at a surface, and v_0 at the outer boundary of the fluid. When this fluid flows along some surface with constant temperature $T_w > T_\infty$, heat is transferred from the boundary to the fluid. Moreover, due to the difference in velocity at the surface, and the outer layer of the moving fluid, a hydrodynamic boundary layer develops, which was described in section 2.1.2 [1]. This layer is represented by the line, between the points **O** and **A** in figure 2.1. Additionally, as heat moves through the fluids, a temperature gradient is created. The temperature of the fluid will then vary between the surface temperature T_w at the surface to the fluid temperature T_∞ at the outside boundary. This is the *thermal boundary layer*, which is represented by the line between points **O** and **B**. Both layers in this case increase with the horizontal distance x. It can also be seen that the thermal boundary layer is thinner than the hydrodynamic boundary layer. This is true for most liquids when the rate

of conductivity is low [1]. As the thermal boundary layer becomes fully developed, the temperature of the fluid is the same as the temperature of the surface, making heat transfer not possible [1].

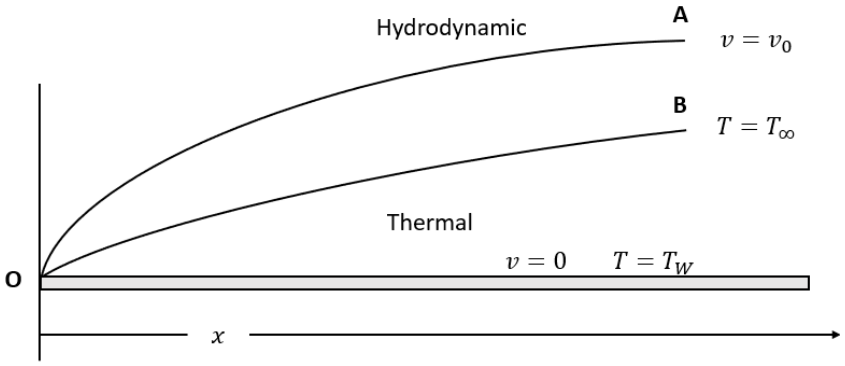

Figure 2.1: Hydrodynamic and thermal boundary layer, inspired by [1].

The ratio of thickness of the hydrodynamic and thermal boundary layer can be described by the Prandlt number *Pr*. The definition for the Prandtl number with flow parallel to a surface is given in equation (2.8). Which is the ratio between the diffusivity of momentum to thermal diffusivity. The hydrodynamic boundary layer and the thermal boundary layer. A Prandtl number equal to 1 would signalize that they are equal, whereas if the number is greater than one the thermal boundary layer is thinner than the hydrodynamic layer. The lower the thermal boundary layer is, the lower rate of conductivity occurs between the fluid and the surface. As conductivity is the mechanism of heat transfer, the fluid needs to be laminar. The Prandtl number also often decreases with temperature as the viscosity of the fluid decreases [1].

$$Pr = \frac{C_\mathrm{p}\mu}{k} \tag{2.8}$$

2.2.4 Nusselt number

The Nusselt number *Nu*, is a dimensionless number that describes the ratio of heat transfer through convection and through conduction which occurs at some surface. As described previously, fluid flow can be laminar, turbulent, or a combination of the two. Different flow regimes, forced and natural convection, and flow geometry will give different variations of Nusselt numbers and other dimensionless numbers. One example of this is the Graetz number for laminar local heat transfer in tubes [1]. The representation for the local Nusselt number for one-dimensional laminar flow is given in equation (2.9). h represents the convective heat transfer coefficient through the surface, with x being the characteristic length, also known as the thickness at which heat transfer through conduction would occur [1].

$$Nu = 0.332\sqrt[3]{\mathrm{Pr}}\sqrt{\mathrm{Re}} = \frac{hx}{k} \tag{2.9}$$

As described the Nusselt number is dependent both on the Reynolds number (2.4) and Prandtl number (2.8).

2.3 Nanofluids and heat transfer

2.3.1 Nanoparticle dispersion stability

Stable particles below 1μm present in a fluid, are known as particle-*dispersion* [27]. The random movement of molecules due to differences in internal energy and collisions is described as *Brownian movement* [28]. The internal movement of particles can influence small particles to form large stable clusters, also known as *agglomeration*. Agglomeration can also occur due to a shear field creating different velocities of the particles, known as orthokinetic aggregation [28]. Both Brownian motion and orthogenetic aggregations alter the collision frequency of particles. The rate of agglomeration is dependent on internally attractive forces, known as Wan Der Waals forces, and repulsive forces, known as electrical double-layer forces [2]. The theory of these attractive and repulsive forces is known as DLVO theory [28]. Gravitational effects on nanoparticles are typically small in comparison to the other forces but will eventually given enough time, ensure the separation of particles and liquid [28]. This process is sped up with the formation of larger structures. When agglomerates reach a certain point, the forces of gravity will become too great and will dominate over other forces. When particles fall to the bottom it is known as *sedimentation* [29].

2.3.2 Nanofluid preparation

There are two main ways to prepare nanofluids, known as the one- and two-step method. As the name indicates, the difference is the number of steps used to synthesize a nanofluid sample. The one-step method synthesizes nanofluids and particles directly in the same process. Whereas in the two-step method, nanofluids and particles are synthesized individually, for so to be mixed together [9]. Most nanofluids are prepared using the two-step method due to the simplicity and economic benefit [9]

A schematic overview of the two-step method can be seen in figure 2.2. The figure also includes some common ways to synthesize nanofluids from the one-step method. However, it should be noted that there are many ways this can be done. Additional routes that can be used for one-step nanofluid synthesis can be found in [3].

There are several ways to increase the stabilization of nanofluids. The most common are the addition of surfactants, sonication, and stirring [9]. There are also other methods that can be utilized, such as calibration of pH levels [30] or surface treatment of particles [31].

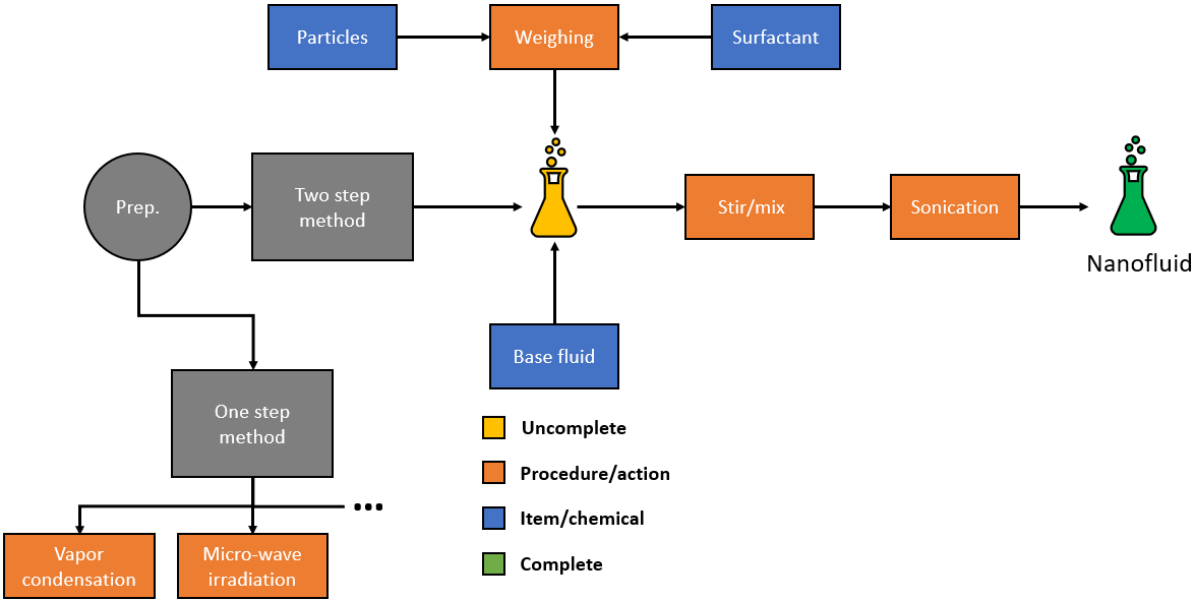

Figure 2.2: Nanofluid preparation method. Figure inspired by [2, 3]

Sonication and stirring

Stirring is done to achieve better dispersion stability of particles in the basefluid and decrease sedimentation. Often a rotating stick in a magnetic field is utilized [2]. Sonication is the use of ultrasonic waves to enhance particle dispersion in the basefluid. The existing agglomerates are subjected to waves, which induce vibration in the aggregated structures. This causes local points of cavitation, breaking the agglomerates down into smaller clusters. Two common technologies are sonic bath and probe-based sonication [2].

Surfactants

Using surfactants is a common method for enhancing nanoparticle suspension [9, 32, 33]. Nanoparticles are either hydrophobic or hydrophilic. Different basefluids are polar or not polar. Both of these factors will decide how easily particles can be suspended in the basefluid. As hydrophilic particles are stabilized by polar liquids (e.g. water), whilst hydrophobic particles are stabilized by non-polar liquids (e.g. oil) [3]. An example of a hydrophobic particle is carbon black.

Water molecules are bound together by hydrogen bonds. When hydrophobic particles are present in a polar medium like water, these bonds will be split as the hydrophobic particle will take up some volume. The polar water molecules will not directly interact with such particles. The molecules affected by the presence of hydrophobic particles will form new hydrogen bonds around the hydrophobic particle. Hydrophobic particles will interact to minimize contact with the surrounding water. When hydrophobic particles aggregate, the structures of water will be broken. Bonding between hydrophobic particles depends on the number of particles, interacting, and agglomerated shape. Additionally, the strength of the bonds will increase with temperature [34].

Surfactants are dispersants that are used to prevent particle clustering. This method is considered to be a cost-effective way of increasing nanofluid stability [2]. Surfactants are made up of a tail and head. In which one end is hydrophobic and the other is hydrophilic. Where one end will attach to the particle and the other to the liquid, increasing the wettability [9]. Even though the addition of surfactants can increase suspension stability, it can also reduce thermal conductivity, leading to foaming, etc. [2, 3]. One example of a surfactant is polyvinylpyrrolidone also known as PVP. It is a polymer made up of long linear groups of 1-Vinyl-2-pyrrolidone and is water solvable [35].

2.3.3 Effective medium theories

Nanofluids offer an additional rate of heat transfer due to the dispersion of particles. This phenomenon has been known since the end of the 19$^{\text{th}}$ century when the characterization of increased heat transfer in fluid-particle suspension was derived in 1873 by James C. Maxwell [36]. Maxwell's relations state that there is a linear increase in conductivity with respect to the particle concentration. The formulation is used to describe the increase in thermal conductivity of fully suspended, non-interacting identical spherical particles. The model, therefore, has some limitations and is best used to describe a low concentration of particles [37]. Which generally mean consecrations of $\varphi < 0.01$ [15]. The formulation is stated in equation (2.10)

$$k_{\text{nf}} = k_{\text{bf}} \left(\frac{k_{\text{p}} + 2k_{\text{bf}} + 2\varphi(k_{\text{p}} - k_{\text{bf}})}{k_{\text{p}} + 2k_{\text{f}} - 2\varphi(k_{\text{p}} - k_{\text{bf}}} \right) \tag{2.10}$$

Where k_{nf} denotes the effective conductivity of the fluid-particle concentration, k_{bf} is the conductivity of the fluid medium and k_{p} is the conductivity of the suspended particle.

Effective medium theories use the average physical properties of both particles and the basefluid as a basis for predicting the increased thermal conductivity [38]. The first effective medium theory was that of Maxwell, presented in the equation (2.10). The model was developed firstly for electrical conductivity [36]. As electrical current and heat flow both must be conserved, the analysis also works for thermal conductivity [38].

A limitation of Maxwell's formulation is often the prediction of thermal conductivity for a larger volume fraction of particles. Bruggeman in 1935 developed a model that takes particle-particle interaction into account. The work was originally done to estimate transport properties for random porous media. The same work can be used to estimate conductivity through porous media (as in materials with particulate materials [39]).

Some other effective medium equations are given in (2.11) and (2.12). Equation (2.11) was developed by Hamilton and Crosser. It is based on Maxwell's equation. However, Hamilton-Crosser takes into account the particle shape as well. Where n is used to describe the shape, in which $n = (3/\psi)$, ψ is the shape parameter, where for spheres

$\psi = 1$ [40]. With a shape parameter for that of spheres, Hamilton-Crosser's model reduces to that of Maxwell. The shape parameter for cubes $\psi = 2$ [41].

$$k_{\mathrm{nf}} = \left(\frac{k_{\mathrm{p}} + (n-1)k_{\mathrm{bf}} - (n-1)(k_{\mathrm{bf}} - k_{\mathrm{p}})\varphi}{k_{\mathrm{p}} + (n-1)k_{\mathrm{bf}} + (k_{\mathrm{bf}} - k_{\mathrm{p}})\varphi} \right) \tag{2.11}$$

The Wasp equation [42] is given in (2.12). This equation is a special case of Hamilton-Crosser and is often used when the shape of the particles is unknown [43].

$$k_{\mathrm{nf}} = k_{\mathrm{bf}} \left(\frac{k_{\mathrm{p}} + 2k_{\mathrm{bf}} - 2\varphi(k_{\mathrm{bf}} - k_{\mathrm{p}})}{k_{\mathrm{p}} + 2k_{\mathrm{bf}} + \varphi(k_{\mathrm{bf}} - k_{\mathrm{p}})} \right) \tag{2.12}$$

The lowest and highest possible bounds of effective properties for two-phase materials with spherical particles were found by Hashin and Shrikman in 1962 [44]. The work was conducted for calculating the magnetic permeability of solid composites, however, it can be used for thermal conductivity due to mathematical similarities [38]. The resulting equation is an inequality (2.13), which confines an interval in which the thermal conductivity must lie. The upper bound is not restricted by the particle volume fraction [38].

$$\left(1 + \frac{3(k_{\mathrm{p}} - k_{\mathrm{bf}})\varphi}{(k_{\mathrm{p}} + 2k_{\mathrm{bf}}) - (k_{\mathrm{p}} - k_{\mathrm{bf}})\varphi} \right) \leq \frac{k_{\mathrm{nf}}}{k_{\mathrm{bf}}} \leq \left(\frac{k_{\mathrm{p}}}{k_{\mathrm{bf}}} \left(1 - \frac{3(1-\varphi)(k_{\mathrm{p}} - k_{\mathrm{bf}})}{3k_{\mathrm{p}} - \varphi(k_{\mathrm{p}} - k_{\mathrm{bf}})} \right) \right) \tag{2.13}$$

The lower bound of (2.13) is actually the same as presented by Maxwell, given in equation (2.10) but in a slightly different form. The reason for this is given as Maxwell's equation is derived for particles that are dispersed perfectly in the medium [38]. The equivalent of this, when regarding thermal resistance, would be a series connection of thermal resistances. Changing between the thermal resistance of the fluid and of the medium [37]. The upper bound of (2.13) would be the equivalent of thermal resistances in parallel. Meaning a continuous connection between particles running parallel to the medium, giving the highest possible thermal conductivity [38].

2.3.4 Possible mechanisms for heat transfer given in the literature

Heat transfer in nanofluids is a complex topic as certain properties are difficult to predict given that multiple factors such as temperature and particle concentration can alter the thermophysical properties of nanofluids [45]. Because of the complexity, some authors like [46, 47] have reported an "anomaly high" thermal conductivity which is not easily explained by effective medium theories such as the Maxwell equation. There is not yet an agreement in the literature on what mechanisms are responsible for the increased heat transfer of nanofluids, compared to the basefluid. However several mechanisms and findings have been reported.

In 2002 a group of researchers, Keblinski *et al.* . [48] proposed that there could be several effects that lead to increased thermal conductivity in nanofluids. Thermal diffusion in nanofluids is stated to occur at a much higher rate than Brownian diffusion. With

this in mind, the authors therefore argue that the increased thermal conduction on account of Brownian motion would be negligible in comparison to the effects of thermal diffusion. The internal thermal resistance can be affected by the creation of small temporary structures, also known as *clusters*. The authors state that the formation of long linear clusters leads to increased thermal conductivity in the fluid. However, long linear structures are improbable. Furthermore, surfactants might further hinder the formation of clusters. Change in thermal resistance at the particle-liquid interface, *Kapitza resistance* is given as another reason for the increased thermal conductivity in nanofluids. The authors argue that the formation of layered liquid at the interface could be the reason. The argument for this is that thermal conductivity is better in a structured medium. Heat is stated to be partially carried by *phonons*, which can be regarded as atomic vibrations [49]. The distance that phonons can travel before they are scattered is called the *mean free path* and is much shorter in unstructured mediums, e.g. liquids than in structured mediums. Therefore an increase in thermal conductivity could occur if a ballistic phonon (Phonons that travel in a straight line between points [50]) can travel to close by (1-2 nm) particles through the fluid.

Some authors have also suggested that Brownian motion is a key component in the increased thermal conductivity of nanofluids, like Jang and Choi [51]. The authors suggest that the effective thermal conductivity of nanofluids can be accurately described by accounting for the conductivity of the basefluid, the thermal diffusivity of particles, and the kapitza resistance. Where the thermal transport from particle collision is neglected. The authors postulate that the Brownian motion produces local convection effects due to the constant interaction between nanoparticles and fluid molecules. As there is no bulk flow, this is said to result in increased conduction at the macroscopic level. A practical analysis of this model is that thermal conductivity strongly depends on the diameter of nanoparticles. The authors found their model to be in good agreement with the measured thermal conductivity of nanofluids containing, copper (Cu), cupric oxide (CuO), and aluminum oxide (Al_2O_3).

Keblinski *et al.* did a review in 2008 [52], where the authors looked at the existing literature of experimental data for nanofluids in order to determine whether effective medium theories could explain the increased thermal conductivity. The authors explain that scanning electron microscopy imaging indicates the existence of chain-like aggregated clusters in nanofluids with high thermal conductivity. The authors explain how different studies are well within the lower and higher bounds of the Hashin and Shrikman inequality given in (2.13). Therefore it is argued that effective medium theory is valid for describing the increased thermal conductivity. The authors suggest that in the case of nanofluids, interfacial resistance does not play a role, as well dispersed nanofluids largely follow the Maxwell relationship. It has also been noted that thermal conductivity increases with temperature and decreasing particle size, as does the probability of the agglomeration rate. The authors therefore conclude that the rate of clustering is the main cause of the increased thermal conductivity. The authors of [38] Support that the effects of nanoparticle clustering could explain the increased heat transfer and that the complex nature of particle aggregation could be the reason for the discrepancy in thermal conductivity in the literature.

Some researchers have also found that aggregated particle size negatively influences thermal conductivity. He *et al.* [53] did an experimental study in 2007. The researchers among other things classified thermal conductivity and rheological properties of 1.0wt.% , 2.5wt.% , and 4.9wt.% titanium dioxide (TiO_2) particles dispersed in water. Particles had an average diameter of 20 nm. Nanofluids were subjected to ultrasonic treatment. The pH was also adjusted to increase stability. The authors found that both viscosity and thermal conductivity were affected by aggregated particle sizes. It was found that the thermal conductivity increased with the particle concentration. Additionally, particle concentration under 1 vol.% could be sufficiently described by Hamilton-Crosser's equation. In this case, the average aggregated particle diameter was 95nm. The authors also studied the change in thermal conductivity with respect to particle size for the sample containing 0.6 vol.% of particles. Here it was found that thermal conductivity enhancement decreased for aggregated particle sizes in the range of 80-210nm. The authors did not discuss the potential reasons for this.

Buongiorno [54] formulated a theory for the increased convective heat transfer which is experienced by nanofluids. The author discusses firstly what develops *slip velocity*, the difference between the basefluid velocity and the absolute velocity of the nanofluid. It is stated that mainly *thermophoresis*, particle diffusion due to a temperature gradient, and Brownian motion will influence the slip. In non-turbulent flow where slip can occur, Brownian motion and thermophoresis may become important. Further, it is stated that the transport in turbulent flow, where slip can not occur, transport is dominated by eddies. Using the discussed slip conditions, and some reasoned simplifications. The author formulates that heat transfer in turbulent flow is because of more movement of particles near the boundary layer at the wall. Convective heat transfer is increased to the thinning and reduction of viscosity of the laminar sublayer due to a lower particle fraction present.

Wen and Ding [55] studied the heat transfer in nanofluids in a laminar flow regime using Al_2O_3 particles suspended in de-ionized water. They found that convective heat transfer was much higher than conductive heat transfer. The authors suggest that increased heat transfer could not only be because of the increased thermal conductivity. As the heat transfer was greater in the entrance region and gradually approached a constant it was attributed to the decrease in the thermal boundary layer. The reason for the decrease in the thermal boundary layer is unknown. The authors however state that one of the possible reasons could be particle migration, shear, viscosity gradient, and Brownian motion at the tube cross-section are given as potential mechanisms for this.

2.4 Cooling of internal combustion engines

Internal combustion engines utilize the chemical energy stored in fuels. As the chemical energy is released it is transformed into heat the pressure of the working medium or gas increases, driving a piston to produce work. There are two main cycles for combustion processes. These combustion processes are spark-ignited combustion (SI) and compression-ignited combustion (CI). A CI-process will often consist of four strokes,

for smaller and medium-sized engines [56]. The ideal diesel cycle can be explained as: 1. Compression, 2. Constant pressure ignition, 3. Expansion and 4.Heat exchange [24].

As the atomized fuel ignites heat is released. This heat warms up the air and other gases to high pressure. When this process occurs inside the cylinder the position piston is usually slightly before the top dead center [23]. The pressure that is generated from the combustion process is used to drive a piston. As a result mechanical work is generated from the release of heat. Energy in an engine is not only transferred through the internal work but also through the cylinder wall but also through the exhaust, phase change of the fuel, and sometimes blow by [56].

The amount of released heat is dependent on many engine parameters. Some examples of this would be *torque* (an engine's ability to do work), *mechanical efficiency* (indicates mechanical energy losses), and *compression ratio* (indication of mechanical energy from fuel). All of these parameters play a vital role in how much heat is generated, and therefore how much cooling must occur in order to maintain an optimal engine temperature [57]. The peak temperature of the burned fuel reaches magnitudes of 2300°C ($\sim$2600K) [57]. The gas pressure and heating cause mechanical, and particularly thermal stress to the surrounding environment [56]. This causes the temperature of the combustion chamber and attached components to increase in temperature. In order to prevent the deterioration of materials due to heat, the surface temperature must be controlled [56]. The cylinder wall temperature must also be controlled for restricting emissions. One example of this is the formation of nitrogen oxide gases (No_x), which form at high temperatures [23].

There are different engine coolants that can be used, depending on the surrounding climate and engine power. Different coolants will have different properties. Some examples of fluids used as coolants are air, ethylene-glycol mixture, water, and oil. The most common for cooling is a mixture of water and ethylene-glycol used. Ethylene-glycol will have a lower freezing point and higher boiling point than water, but a lower thermal conductivity. Glycol is also a fluid that is sheer thinning which makes the viscosity lower with an increased shear rate. Waters viscosity on the other hand is independent of shear rate [56]. Coolant viscosity is an important factor, not only is the thermal conductivity and rate of natural convection important for heat transfer. But an increased viscosity will also lead to more friction losses of the fluid, which is then responsible for the pressure drop and required pumping power [58]. Which can potentially lead to self-heating [1].

Heat transfer in engines is a complex phenomenon, where changes occur rapidly. Lots of factors can influence heat transfer. In addition to the conditions mentioned earlier in this section; coolant density, velocity, heat capacity, component geometry, and thermal load will also play a role. Moreover, nucleate boiling and cavitation due to engine vibrations can also be a cause of locally variable heat transfer throughout the engine [56]. Cooling of the cylinder wall is traditionally mostly dominated by forced convection. In the area of direct contact between the cylinder wall and the coolant, there will be some heat transfer through conduction as the flow of the thermal boundary layer must be laminar. However, cooling through conduction and radiation is often negligible in

comparison to convection [56].

2.5 The use of nanofluids in thermal cooling systems

Heat transfer is a popular suggested area for nanofluids, as they often inhibit properties like increased rate of thermal conductivity [59]. This section will present some of the uses within cooling applications of nanofluids from the literature. Nanofluids have been suggested to be used as engine coolants. The reason for this is that an increased heat transfer in coolant systems could potentially reduce the size of coolant systems. The following section will therefore review some of the literature on the use of carbon black compared to other types of particles. As well as what type of engine cooling applications nanofluids are used for.

2.5.1 Carbon black nanofluids

When it comes to heat transfer applications, most of the literature has taken to using metal oxide particles [60, 61, 62, 63, 64] or metal particles [65, 66]. It can also be seen that the use of certain carbon-based nanoparticles, e.g. carbon nanotubes [67, 68] have been studied. The basefluids of these studies are mostly either water or ethylene-glycol. Regarding carbon black particles, which has been used in this thesis, most application in the literature are predominantly for solar thermal technology [69, 70, 71] due to their ideal properties for light absorption.

There are however some studies present, in which heat transfer and other thermophysical properties are the main focus. In a 2011 paper, Meng *et al.* [72] studied the rheological behavior, photo-thermal properties, and thermal conductivity of carbon black particles in ethylene-glycol, using PVP to enhance particle suspension. Clusters were measured to be in ranges of approximately 88-148 nm. The authors noted an increased thermal conductivity, with temperature and the highest rate of thermal conductivity for 7.8wt.% of particles which had an increase of about 15% from the basefluid. The lowest increase was for 2.2wt.% particles, which had a relative increase of 4%. All fluids had shear thinning behavior. Larger concentrations of carbon black had higher initial viscosity but higher rates of sheer thinning.

Ukei *et al.* [30] investigated the thermal conductivity of carbon black and carbon nanopowder suspended in water for 0.5, 1, and 1.5 vol.% particles using PVP. The nanofluids were made with 0.5wt.% of PVP. Stability was also affected by altering the pH. The authors took measurements of heat capacity and thermal conductivity. Heat capacity was measured using the temperature increase of the liquid due to electric heating in an adiabatic environment. The measurements of thermal conductivity were measured using a transient hot wire and compared to Maxwell's and Hamilton-Crosser's equations. The authors found that the particles using carbon black could be estimated using the Hamilton-Crosser's equation, and were slightly larger than Maxwell's equation. Both instances of thermal conductivity were found to be within the bounds given

by Hashin and Shtrikman. Carbon nanopowder was found to have a higher thermal conductivity, but a lower specific heat capacity. The increased thermal conductivity is thought to be from particle agglomeration at the transient wire. The carbon black fluid was found to have a relative increase to water at 7%, at 1.5 vol.% particles.

Some have also looked at carbon black for heat transfer applications. One of these is Shivari *et al.* [73] which did a recent experimental study, where the authors investigated the convective heat transfer of a coiled heat exchanger and entropy generation. The nanofluids used were for 0.1, 0.2, and 0.4wt.% carbon black concentration, with the addition of an SDS ratio of 1:1 for increased suspension stability in water. The fluids were sonicated for 30 minutes. The authors measured the temperature difference and pressure drops at various points in the fluid. The experimental setup consisted of an electrical pump, which pumped liquid at a rate of 3-7 liters per minute from a 25-liter tank. The heater used a 1500 W electrical element. The fluid was considered to be fully turbulent. It was found that the Nusselt number ascended, with an increase of the Reynolds number multiplied by the Prandtl number. The liquids with the highest Nusselt numbers were 0.2wt.% and 0.3wt.% carbon black concentration. Whereas 0.4wt.% carbon black concentration performed slightly better than pure water. As the Nusselt number is related to the heat transfer coefficient, this would say that 0.2% has the highest rate of heat transfer. It was found that at optimal conditions this concentration could have a heat transfer coefficient which is 14.8% greater than that of water. The highest recorded heat transfer coefficient at $Re = 31 \cdot 10^3$ was 1014.53W/m·K. It was also found that friction losses decreased with an increase in Reynolds number.

2.5.2 Nanofluids application in engine radiator

From the literature, it can be found that a popular research area for nanofluids in engine cooling, is for the engine radiator with both theoretical and experimental studies. The following section will provide some examples of this.

Several authors have investigated the possibility of using nanofluids in engine radiators. Goudarzi and Jamali [74] investigated heat transfer in a car radiator of Al_3O_2 with a volume concentrations less than 1% in ethylene glycol. The authors found that using coils on both sides of the radiator, with nanofluids gave an increased heat transfer of 5%, compared to the basefluid. Sharma [75] looked at the possibility of using Aluminium particles of 0.2 and 0.3 vol.% in distilled water as a way to increase heat transfer in a car radiator. The author found substantially increased thermal conductivity with an increase of 38% at 67°C . The author also found that 0.3% particles gave the highest increase in heat transfer in the heat exchanger by 23.6% compared to the basefluid. Further examples of experimental studies are Peyghambarzadeh et al, which investigated the use of Al_3O_2 in a car radiator dispersed in water [76] and ethylene glycol [77].

Regarding theoretical studies, the authors of [78] investigated the use of 2% copper particles dispersed in ethylene-glycol in a car radiator. The paper found that the radiator became more effective using nanofluids. With an increased rate of 1.4% increase in

heat transfer with coolant Reynolds number of 40000. Further examples are Delavari and Hashemabad which did a computational fluid dynamics (CFD) analysis of both turbulent and laminar flow in a car radiator [79]. Hussein et al did a numerical analysis of turbulent flow in a car radiator [80].

2.5.3 Nanofluids in direct engine application

Some studies have done research on the direct application in combustion engines with nanofluids. Some researchers have studied the possibilities of using nanoparticles in engine oil, like Tzeng *et al.* or Kumar *et al.* [81, 82]. Whereas others have studied nanofluids as direct engine coolants, though it has proven difficult to find easily available and relevant examples of this.

The authors behind [83], Michali *et al.* , investigated whether nanofluids could be a viable solution for offsetting peak engine temperature in a single-cylinder four-stroke CI engine. The study used CuO suspended in water. Temperature sensors were mounted at several different locations in the engine head. The nanofluid coolant was tested for thermal conductivity at 20°C using a transient hot wire. it was found that the thermal conductivity could be described using Hamilton-Crosser's equation. There was conducted seven different tests. Two tests using water. Two tests used 1.4 vol.% particles and three tests used 2.5 vol.% particles. The authors tested both under transient and steady-state conditions. The tests used 15 liters of coolant. It was found that the temperature changes of the engine block were dependent on the engine load. At 25% engine load, the effects of nanofluid were negligible compared to water, whereas the highest reduction of temperature was found at full engine load. This effect was best noticed at the exhaust valve seat and spindle with a reduction in the temperature of 4.1% and 13.6% at these locations respectively under transient loads compared to water. under steady-state conditions, this reduction was found to be 1.4% and 12.5% compared to water. In both cases, 2.5 vol.% nanofluid was used.

Muruganandam and Kumar [84] did a study in 2020 in which the authors investigated whether different concentrations of 0.1, 0.3, and 0.5 vol.% multi-walled carbon nanotubes in distilled water could be utilized as an engine coolant. The nanoparticles were stabilized with sodium do-decyl butane sulfonate (SDBS) and an ultrasonic bath. The engine that was used was a single cylinder four stroke 3.7 kW diesel engine. At full load, the engine's torque was 24 Nm. In order to quantify the nanofluid enhancement of heat transfer. The authors used thermocouples placed at various locations e.g. for the inlet and outlet temperature of the coolant, and a flow meter. It was found that the highest mechanical efficiency achieved was using the 0.3 vol.% nanofluid coolant. Respectively to water, the different concentrations resulted in an enhancement of 8%, 18%, and 16% for 0.1, 0.3, and 0.5 vol.% particles. This effect also resulted in a reduction in specific fuel consumption. For 0.3% particles, it could be seen that specific fuel consumption varied between 9 and 19% compared to water, depending on the engine load. The exhaust gas temperature also saw a similar trend.

The present literature study goes through some of the available literature regarding the use of carbon black nanoparticles and the uses of nanofluids for heat transfer applications with respect to thermophysical properties. As well as the use of nanofluids in combustion engines. From the available literature, it can be seen that heat transfer of nanofluids is a popular research subject, with a focus on the use of metal-oxide particles. This thesis has decided to use carbon black as nanoparticles, which can be seen in the literature predominately studied in solar thermal systems. Further, it was found that the use of nanofluids for direct engine cooling is underrepresented in the literature compared to the use of nanofluids in car radiators. As this work seeks to understand whether carbon black could potentially be used as an engine coolant, it will provide data for an area of research that, as of today is not developed.

Chapter 3

Methods

This chapter will review the methods that were used in order to derive the results that are presented in chapter 4. In order to effectively determine whether carbon black-nanofluids can offer any benefit to be used as an engine coolant, it is important that the work is repeatable.

The work in this thesis was carried out in three main parts. Figure 3.1 gives an overview of the work carried out in it is entirety. More information about the specific processes can be found throughout the following chapter. The first step includes preparation. This was important as many different surfactants and particle composition were tested. Once a suitable fluid profile was determined, testing of physical properties could be carried out. At this point, testing of viscosity and stability was the main focus, with fluids found in the preparation phase. The final phase contains the processing of the data collected in step two. Additionally, the experiment with the engine was designed and carried out.

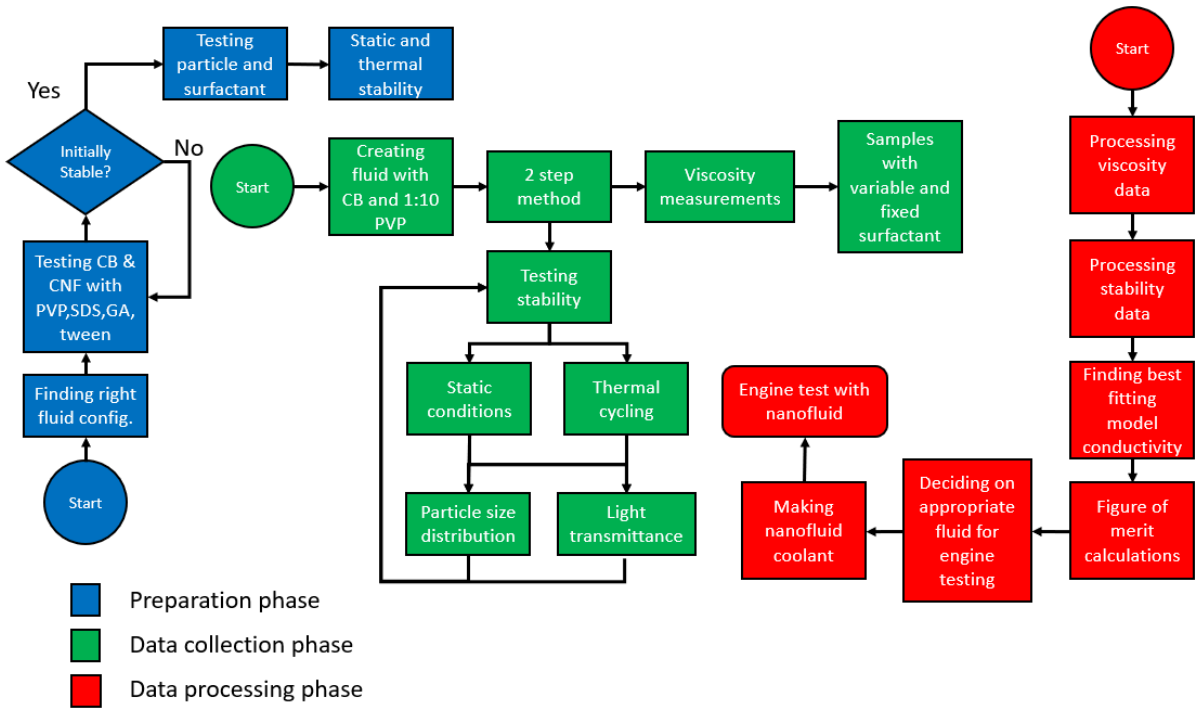

Figure 3.1: Description of the work process

3.1 Nanofluid preparation procedure

Nanofluids were prepared using the two-step method as illustrated in figure 2.2. This is the most common approach for making nanofluids but does however lead to greater rates of sedimentation [9, 2]. The measurements were done with an AG204 scale from Metler Toledo. All created samples contained 100g of liquid. Finding the most optimal solution of surfactant, particle type, particle concentration, and treatment was an iterative process where all the parameters above were tweaked in order to achieve sufficient stability. Both ENSACO 350G carbon black with a nominal diameter of 50nm from Timcal and carbon nanofibers with a diameter of 100-500 nm were considered as possible choices. Surfactants considered were polyvinylpyrrolidone (PVP), sodium dodecyl sulfate (SDS), gum arabic, and Tween20. All surfactants were tested for both types of particles. Particle concentrations were studied for 1wt.% , 2.5wt.% , 5wt.% , 7.5wt.% , and 10wt.% . Different types of water were experimented with, this included: tap water, de-ionized water, and de-mineralized water. As there was no noticeable difference between the different types of water, tap water was chosen as the basefluid. The tap water which was used in this work had a pH of 7.56, measured with a PEN pH-meter: pH-223 from LTT Lutron. Different particles, particle sizes, and geometry might give different results than what is obtained in this thesis.

It was found that a 1:10 ratio wt. of PVP to carbon black particles gave the most stable nanofluids. Both carbon black as nanoparticle [70, 69] and PVP as surfactant [85, 86] are studied in the literature. PVP is a polymer that dissolves in water [87]. The PVP used in this work was acquired from Thermo Scientific. All samples were mixed by hand so that the surfactants, particles, and basefluid became a single multi-phase liquid. The amount of mixing required depended on the particle and surfactant concentration. All liquid samples were sonicated for one hour using an ultrasonic probe. Ultrasonic treatment is a common way for enhancing stability [88]. Treatment for one hour was chosen in order to ensure a breakdown of particle agglomerates as the literature has not established an ideal sonication time for different concentrations [60]. However, [89] found that sonication of Iron (Fe) nanofluids for 50-70 minutes had a higher thermal conductivity than shorter sonication times. The probe is of the type ultrasonic homogenizer MEF93.T from MELFIZ (Moscow, Russia). Ultrasonic treatment of the samples took place at 600 W power and 22 $\pm$1,65 kHz.

The required amount of fluid for the engine test was estimated to be 7 kg. For this purpose, it was chosen to use 2.5wt.% and 0.5wt.% of particles based on the results presented in chapter 4. This meant that the sample size by using a sonic probe would not be sufficient. Instead, a sonic bath from Biltema, designed for the use of larger volumes was used. Sonic baths however produce a lower intensity and unevenly distributed vibrations, making them less effective [60]. In order to produce enough coolant, 5kg of liquid was produced in a 10-liter plastic tank and placed in the sonic bath. The sample consisting of 0.5wt.% were sonicated for 1 hour, whereas the 2.5wt.% sample was sonicated for 2 hours in order to disperse the particles. Treatment was done with 240W power at 240kHz. The tank was shaken thoroughly every 20 minutes to ensure proper mixing. After this was completed, an additional 2kg was prepared in the same manner.

3.2 Fluid characteristics

The different fluids were studied with respect to stability, viscosity, and thermal conductivity. More about the measurements can be read in this section. The density of each sample was calculated using the mass-to-volume fractions of each component. The relation is given in formula (3.1) from [90].

$$\rho_{\mathrm{nf}} = \frac{m_{\mathrm{nf}}}{V_{\mathrm{nf}}} = \frac{m_{\mathrm{p}} + m_{\mathrm{bf}}}{V_{\mathrm{nf}}} = \frac{V_{\mathrm{p}}\rho_{\mathrm{p}} + V_{\mathrm{bf}}\rho_{\mathrm{bf}}}{V_{\mathrm{nf}}} = (1-\varphi)\rho_{\mathrm{bf}} + \varphi\rho_{\mathrm{p}} \tag{3.1}$$

The different subscripts nf, p, and bf represent nanofluid, particles, and basefluid respectively. Where m represents the mass, V represents volume, ρ represents the density and φ represents the volume fraction of particles $\varphi = \frac{V_{\mathrm{p}}}{V_{\mathrm{nf}}}$.

The Volume fraction of the particles was calculated via the mass fractions by equation (3.2)

$$\varphi = \frac{V_{\mathrm{p}}}{V_p + V_{\mathrm{bf}}} = \frac{\frac{m_{\mathrm{p}}}{\rho_{\mathrm{p}}}}{\frac{m_{\mathrm{p}}}{\rho_{\mathrm{p}}} + \frac{m_{\mathrm{bf}}}{\rho_{\mathrm{bf}}}} = \frac{m_{\mathrm{p}}}{m_{\mathrm{p}} + m_{\mathrm{f}}\frac{\rho_{\mathrm{p}}}{\rho_{\mathrm{bf}}}} = \frac{x}{x + \frac{\rho_{\mathrm{p}}}{\rho_{\mathrm{bf}}}} \tag{3.2}$$

In which x denotes the individual mass fraction. The specific heat capacity under constant pressure for the nanofluids, C_{p} was calculated for all concentrations with equation (3.3). The equation has previously been shown to accurately predict heat capacity from [91]:

$$C_p = \frac{\varphi\rho_{\mathrm{p}}C_{p,\mathrm{p}} + (1-\varphi)\rho_{\mathrm{bf}}C_{p,\mathrm{bf}}}{\varphi\rho_{\mathrm{p}} + (1-\varphi)\rho_{\mathrm{bf}}} \tag{3.3}$$

An overview of the calculated properties for the nanofluids with variable concentrations of PVP can be seen in table 3.2. In order to use the equations (3.1), (3.2), and (3.3) certain parameters needed to be estimated. These parameters and values are listed in table 3.1, with the value's origin.

Some assumptions have been made for certain fluid characteristics in the temperature range of 20 and 90°C . This includes that the heat capacity for water is constant, and density, heat capacity, and thermal conductivity for carbon black particles are constant. Moreover, the increase in density due to PVP is thought to be negligible, and not alter the heat capacity when dispersed in water. It is expected that variations in heat capacity are small enough to be neglected with an increase in temperatures. Table 4.4 in chapter 4 show how temperature will influence the properties of the different concentrations.

Relative thermophysical properties were used in order to determine the change in some properties e.g. viscosity of nanofluids, compared to the base value of e.g. water. The relation is given in (3.4). Where x denotes the studied property.

$$x_{\mathrm{r}} = \frac{x_{\mathrm{nf}}}{x_{\mathrm{bf}}} \tag{3.4}$$

Table 3.1: Calculation parameters

Parameter	Value	Unit	Description	Origin
ρ_p	$1.86 \cdot 10^3$	$\frac{kg}{m^3}$	Particle density	[92]
ρ_w	998-950	$\frac{kg}{m^3}$	Water density at 20, 50, 70 and 90°C	[24]
ρ_{EG}	992, 983	$\frac{kg}{m^3}$	EG density at 40 and 60°C	[93]
$C_{p,p}$	0.71	$\frac{kJ}{kg \cdot K}$	Particle specific heat at 20°C	[83]
$C_{p,w}$	4.2	$\frac{kJ}{kg \cdot K}$	Water specific heat at 20°C	[24]
$C_{p,EG}$	2.474, 2.562	$\frac{kJ}{kg \cdot K}$	EG heat at 40 and 60°C	[24]
k_p	129	$\frac{W}{m \cdot K}$	particle thermal conductivity at 20°C	[94]
k_w	0.598-0.673	$\frac{W}{m \cdot K}$	thermal conductivity of water at 20,50,70,90 °C	[1]
μ_w	1.0-0.314	mPa · s	Water viscosity at 20,50,70,90 °C	[1]
d_{H_2O}	0.265	nm	Diameter of a water molecule	[27]
d_p	50	nm	particle diameter	Manufacturer

Table 3.2: Calculated nanofluid properties, with 1:10 ratio of PVP for 20°C .

CB(wt.%)	Volume-fraction(φ)	Density (ρ)/$\frac{kg}{m^3}$	Heat capacity(C_p)/$\frac{kJ}{kg \cdot K}$
0	0	998.19	4.2
0.5	0.0027	1000.496	4.183
1	0.0053	1002.790	4.165
2.5	0.0132	1009.599	4.115
5	0.0261	1020.711	4.034
7.5	0.0387	1031.535	3.957
10	0.0509	1042.084	3.883

3.2.1 Stability

part of the characterization of properties was to determine stability. This was done in order to ensure that the chosen nanofluid compositions would be suitable as an engine coolant. Two types of stability were investigated for different particle concentration nanofluids. Stability included static long-term stability and thermal stability as the nanofluids were to be used under high temperatures. Each sample from 0.5wt.% -10wt.% of 100g was divided into two parts of 50g. One set was used to determine static stability, and one set to determine thermal stability.

Thermal stability was investigated by *thermal cycling*. The procedure was carried out by placing the six samples in a circular position. Using an aluminum plate for even heat distribution, on top of an electric hot plate. The plate's power was set between 1000 and 1250W. All six samples were rotated by one to the left, each cycle. This was done due to reduce the influences of an imbalanced thermal load. For each thermal cycle,

the samples were kept between 90 and 100°C , for 10 minutes. The samples were then water-cooled back to room temperature. The temperature of the samples was controlled using an RS-42 thermometer with a K-element which was placed into two of the samples. In this work, the temperatures of samples with 2.5wt.% and 7.5wt.% carbon black were controlled. The temperature was controlled for the same samples for all 30 cycles.

Static testing was done with the other corresponding 50g of liquid. The samples were placed at rest, with little external interference. After every 10 cycles for the cycled samples, and every week for the static samples, a small amount of liquid was removed so that the particle density and particle size distribution (PSD) could be tested using dynamic light scattering and Ultraviolet (UV) visible spectroscopy.

3.2.2 Dynamic light scattering

The particle size distribution and average aggregated particle diameter were measured using a Malvern Mastersizer 2000 system. The output data from the Mastersizer require no further major modification. PSD using dynamic light scattering (DLS) is a common way of quantifying particle sizes [95, 66]. Using light scattering, the Malvern Mastersizer calculates average particle size and particle distribution which are fitted to a distribution curve [66]. Each sample underwent 3 measurements, where the average values were used. This procedure was integrated into the system. Each sample was shaken to redistribute sedimented particles before each measurement.

The Malvern uses aqueous solutions as a dispersant. Which makes it possible to analyze the PSD of nanofluids. Bubbles of air can form in the liquid. The system measures these bubbles as particles. It is stated in the user manual that measurements can be influenced by air bubbles. This is typically characterized by a separate measurement peak around 100μm [96].

3.2.3 Ultraviolet visible spectroscopy

Ultraviolet (UV) visible spectroscopy is a common method for evaluating particle concentration density [97, 98]. The rate of absorption is linearly proportional to the concentration of particles present in the fluid sample [9]. This work used a UV-5100 spectrophotometer from Metash. UV visible spectroscopy was used in order to evaluate the dispersion stability of the nanoparticles in the basefluid. Values were measured each week and after every 10^{th} cycle. In order to compare values, an extinction coefficient was calculated using uniform Beer-Lambert law as can be seen in equation (3.5).

$$T = -\frac{1}{d}\ln(10^{-A}) \tag{3.5}$$

Where T is the value of the transmittance coefficient, d is the thickness of the liquid and cuvette, the light will travel through, and A is the absorbance which is outputted from the measurement system.

The measurements procedure was done by diluting nanofluid in 10g of water using a mechanical pipette, set for 10 μl. For concentrations of 0.5wt.% carbon black 30μl was diluted, for 1wt.% carbon black, 20μl was diluted, and for the rest 10μl was diluted. This was done in order to ensure an absorbance coefficient between 1 and 2.5. After the samples had the right dilution about 3.6g of liquid was placed into a cuvette to be analyzed. Light was transmitted at wavelengths between 300-750nm.

3.2.4 Electron microscopy

Electron microscopy was done in order to characterize the geometry of particles and particle agglomerates. The images were taken of a diluted sample of nanoparticles dispersed in water with PVP. The samples contained 0.1wt.% carbon black and 0.05wt.% PVP. This ratio was chosen as it was known to be stable from earlier experiments. The samples were created with the same method described in section 3.1. The images were taken using non-coated silica wafers in the Zeiss Gemini 450 scanning electron microscope at the University of Bergen's ELMILAB. More information about the lab can be found here [99].

3.2.5 Rheological study

Viscosity measurements were carried out using an NDJ-8S viscometer which is a spindle and cylinder-based meter. The viscosity is calculated via the shear rate. All measurements used the number 0 spindle and cylinder for rational speeds of 6, 12, 30 and 60 rpm. Due to accuracy readings, only 60 rpm has been considered a reliable result. Additional information about the device can be found in the user manual [100]. Another viscometer was used to verify the results presented in figure 4.6. This ball-viscometer used is of the type Anton Paar Lovis 2000ME.

Viscosity was measured for different basefluids and nanofluids. This was done in order to gain an understanding of how particle concentration and surfactant would influence viscosity. Table 3.3 gives an overview of the studied samples. The table consists of three sets. Set 1 contains the fluids that were considered as coolants, with a 1:10 ratio of PVP to particles. Set 2 was used to understand how particle concentration would affect the viscosity, with a constant PVP level. Set 3 has been studied to see how PVP influences viscosity in water, which is the nanofluids basefluid. This set contained no particles. Each sample was measured 20 times for each rotational speed with a 30-second time increment between the recording of each value in ascending order with respect to concentration. The average of these 20 measurements was further used to indicate viscosity. The standard deviation from these measurements was calculated by equation (3.17). The measurement cell and spindle were rinsed after each measurement to avoid sample contamination.

Additionally to measuring the viscosity, some selected equations were tested to see if they could adequately capture the measured data. One of the equations that were used was Einstein's viscosity equation as given in (2.2). The second model is that of Brinkman's model given in equation (2.3). Which are both common theoretical mod-

Table 3.3: Viscosity studied samples

Set 1		Set 2		Set 3	
PVP (wt.%)	**CB (wt.%)**	**PVP(wt.%)**	**CB (wt.%)**	**PVP (wt.%)**	**CB (wt.%)**
0.05	0.5	0.5	0	0.05	0
0.1	1	0.5	1	0.1	0
0.25	2.5	0.5	0.25	0.5	0
0.5	5	0.5	5	0.75	0
0.75	7.5	0.5	7.5	1	0
1	10	–	–	1.25	0
–	–	–	–	2.5	0
–	–	–	–	3.75	0

els [20].

3.2.6 Thermal conductivity

Measurements for thermal conductivity were not available until after the particle concentration of the coolant was decided. This was due to a lack of measurement equipment. As an alternative, several models were reviewed to the measured thermal conductivity provided by Grebstrad [4]. The author among other things, investigated the thermal conductivity of the same particles used in this thesis. The difference however is that Grebstad used SDS as a surfactant and not PVP. It was assumed that thermal conductivity will vary little between different surfactants [101]. Four data points were collected from Grebstad for the thermal conductivity of nanofluids containing 0, 0.5, 2, and 4wt.% of nanoparticles.

Theoretical models

Due to the initial lack of measurement equipment, finding an adequate theoretical model was chosen as an alternative. Different authors have found that mean field models can be used to accurately describe the thermal conductivity of nanofluids [102, 103].

Several equations were considered. The final equations that were used were used were Maxell's model (2.10), Hamilton-Crosser's model (2.11), and Wasp's model (2.12). The shape parameter was set to 1.5 when using Hamilton-Crosser's equation. This was done in order to estimate "rough" spheres and to see how the particle shape would influence the thermal conductivity of nanofluids. These three models are part of what is often described as effective medium or classical models of thermal conductivity for nanofluids [104]. In addition, a newer equation was also included from Prayazhnikov (3.6), which was derived in 2017 by Pryazhnikov *et al.* [105]. The authors found the equation to give accurate results within 3wt.% of nanofluids with different proper-

ties, such as particle size, particle type, and concentration to list a few.

$$k_{\mathrm{nf}} = k_{\mathrm{bf}} \left((1 + 0.0193 + 0.00383) \left(\frac{\rho_{\mathrm{p}}}{\rho_{\mathrm{bf}}} \right) \sqrt{\varphi \left(\frac{d_{\mathrm{p}}}{d_{\mathrm{w}}} \right)} \right) \tag{3.6}$$

Where d_{p} and d_{w} is used to denote nanoparticle diameter and basefluid molecule diameter respectively.

Experimental testing

Experimental testing of thermal conductivity occurred after the fluid had been decided for the engine testing. A transient hot wire THW-L2 from Thermtest was used. This method is ideal as it can be done quickly, and neglects heat transfer due to convection [106]. Six concentrations were tested that had earlier had been studied for stability under static load were re-sonicated for 40 minutes. This was done in order to break up the particle agglomerates. First, the thermal conductivity meter was tested against known values of de-ionized water at 20°C and 50°C . The respective thermal conductivity is supposed to be 0.598 $\mathrm{W/m \cdot K}$ and 0.640$\mathrm{W/m \cdot K}$. These measurements were conducted 5 times and showed an error from the expected value of $\pm 0.583\%$ and $\pm 3.885\%$ respectively. The error was calculated through the standard deviation in equation (3.17).

Each measurement used 15 ml of liquid and was tested five times at 21°C . The transient hot wire and measurement cell was rinsed after each measurement to avoid sample contamination. The temperature was controlled using an Echotherm chilling/heating dry bath. Thermal conductivity was tested for water and PVP solutions and nanofluids as done for viscosity set 1 and 3 in ascending order with respect to the concentration. This was done to see how the thermal conductivity of the nanofluids and their base changed.

3.3 Engine system

The engine that was used is a single-cylinder water-cooled 1965 Petter diesel 6 kW engine. It is given in the engine manual that coolant temperature should not exceed 82°C and deceed 60°C . The description is given as the pipes should be too hot for touch, but not so hot that the coolant is boiling. The engine radiator is limited to 5.1 liters. The cooling geometry of the cylinder is unknown, however, an estimate of coolant volume around the cylinder walls was to be 1.778 liters. A potential plug of the coolant flow could cause problems for the engine however the diameters of the valves and pipes were found to be not an issue with regards to clogging. A schematic overview of the test setup can be seen in figure 3.2. The subscripts i and o represent in and out of the engine, respectively. T is given for temperature, $\dot{W}$ for electrical power, $\dot{Q}$ for thermal power, $\dot{V}_0$ for the volumetric flow externally to the heat exchanger and $\dot{V}_1$ for the volumetric flow of coolant. The blue and red thick lines illustrate cold and hot coolant, respectively. Tests took place at pressures of approximately 1 atmosphere.

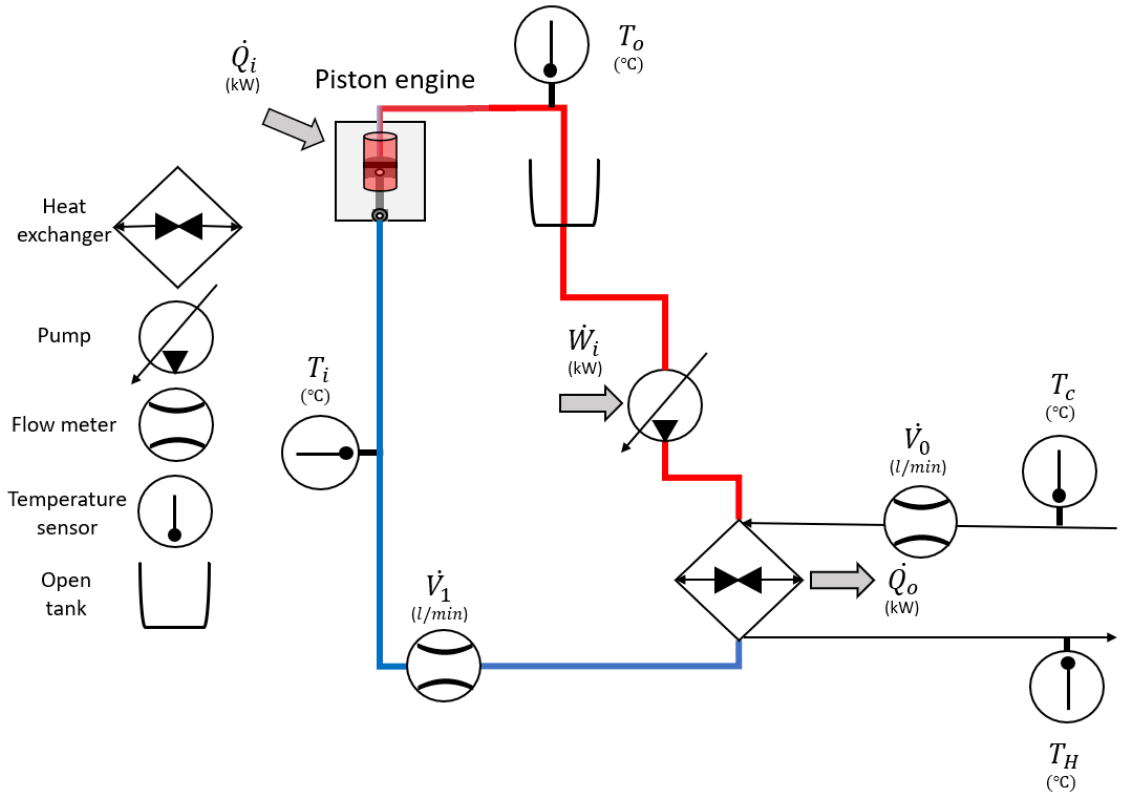

Figure 3.2: Engine test schematic setup

3.3.1 Test procedure

Several tests were carried out. The specifications for each test procedure are in table 3.4. All tests were conducted with an engine load of 20Nm and 1500 rounds per minute (rpm). The external flow denoted $\dot{V}_0$ from figure 3.2 was not altered between tests. This flow was measured with a coriolis Flow Meter. The heat exchanger that was used is a liquid-to-liquid heat exchanger. The heat exchanger's liquids were at the time tested with engine coolant and water that came from the external circuit. The water in the external circuit had an average inlet temperature $\bar{T}_c$, of 31°C with little deviation. The average difference in temperature was approximately 3.5°C . The average volumetric flow of the external circuit was registered to be $\bar{\dot{V}}_0$ = 12.7 ±0.3 liter/min. The temperature sensors that were used were RS type K Thermocouple.

Table 3.4: Engine testing

Test	Liquid	Description	$\dot{V}_1/(\frac{l}{min})$	Function
1	Ethylene-glycol (EG) and water	20 vol.% EG in water	3,4,5	Reference
2	Water	100% water	3,4,5	Reference
3	Nanofluid	0.5% CB & 0.05% PVP	3,4,5	Nanofluid coolant
4	Nanofluid	2.5% CB & 0.25% PVP	3,4,5	Nanofluid coolant

3.3.2 Calculation of heat transfer to coolant

Data was logged in a comma-separated value (CSV) format every 10 seconds. The flow measurement at certain times provided an incorrect value, showing negative or zero flow. A Python library called numpy was used to avoid these measurements influencing the average flow. This was done by replacing all values below or equal to the minimal achievable flow of 1.9 liter/min with an empty value (nan). From there, numpy offers several functions for working with nan values [107]. An example showing different plotted values from the raw data can be seen in Appendix A

Each coolant was logged in a separate file. For each volumetric flow value (3, 4& 5 liter/min) in each file, an interval was found where the flow and temperature gradient was approaching zero. Meaning that the values were more or less stable. This was done to avoid the influence of changes in the coolant regime. An average value of the difference in temperature in and out of the engine, ΔT was calculated from the stable interval. The heat transfer to the coolant $\dot{Q}$ was calculated through the temperature difference, mass flow, and heat capacity given in equation (3.7) from [1]

$$\dot{Q} = \mathrm{C}_p \dot{m} \Delta T = \mathrm{C}_p \rho \dot{\dot{V}} \Delta T \tag{3.7}$$

As the densities are given in kg/m^3 in table 3.1, the volume flow was converted from liter/min to m^3/s. Heat capacity and density were selected for 50°C . The deviation of both the density and heat capacity between the lowest and highest possible temperature is less than one percent for all coolants. Therefore, these properties were assumed to be constant with temperature. The heat capacity for pure EG was found using linear interpolation with values provided in table 3.1, as given in equation (3.15). The heat capacity of the EG and water mixture for test 1 in table 3.4 were found by adding the heat capacities of water and EG multiplied with the individual volumetric fractions of 0.8 and 0.2 respectively.

3.4 Theoretical relations

3.4.1 Figure of merit

For coolants, different parameters, such as density, viscosity, and thermal conductivity are decisive factors for how effectively heat can be transferred, and how easy it is to internally pump the coolant. Therefore several theoretical relationships have been created in order to describe the effectiveness of a coolant. One of these relationships has been described as a figure of merit (*FOM*). This is a theoretical measurement of how effective cooling or heating will occur, using a particular fluid. This is done by finding changes in the relative thermophysical properties of nanofluids to some relative fluid, here denoted by subscript "bf". If the FOM is greater than 1, it means that the nanofluid has a higher cooling efficiency than the relative fluid, which in this case is water.

Many FOM equations are based on the Mouromtseff number, Mo [108]. Which is given in the form of equation (3.8). Where a,b,d and e are coefficients that vary, depending on the application and derivation.

$$Mo = \frac{\rho^a k^b C_p^d}{\mu^e} \tag{3.8}$$

The Mo have visual similarities to other relationships, such as the Reynolds number Re with the exception that the Mo is not dimensionless. Several FOM equations have been developed using Mo. Some of these have been used in this work in order to gain an understanding of the optimal concentration. One of the equations used was (3.9) by Vajiha and Das (V-D) [45]. The equation is used for fully developed turbulent flow. It relates the forced convective heat transfer h of the nanofluid to the relative fluid.

$$FOM_{\text{V-D}} = \frac{Mo_{\text{nf}}}{Mo_{\text{bf}}} = \frac{h_{\text{nf}}}{h_{\text{bf}}} = \frac{k_{\text{nf}}}{k_{\text{bf}}} = \frac{\rho_{\text{nf}}^{0.8} k_{\text{nf}}^{0.5} C_{p,\text{nf}}^{0.5}}{\mu_{\text{nf}}^{0.3}} \frac{\mu_{\text{bf}}^{0.4}}{\rho_{\text{bf}}^{0.8} k_{\text{bf}}^{0.6} C_{p,\text{bf}}^{0.5}} \tag{3.9}$$

Yu *et al.* [90] determined the constants for a fully developed internal turbulent flow heating and cooling, based on the fanning friction factor. The equations are described respectively in (3.10) and (3.11).

$$FOM_{\text{Heat}} = \left(\frac{\rho_{\text{nf}}}{\rho_{\text{bf}}}\right)^{0.8} \left(\frac{C_{p,\text{nf}}}{C_{p,\text{bf}}}\right)^{0.4} \left(\frac{\mu_{\text{bf}}}{\mu_{\text{nf}}}\right)^{0.4} \left(\frac{k_{\text{nf}}}{k_{\text{bf}}}\right)^{0.6} \tag{3.10}$$

$$FOM_{\text{Cool}} = \left(\frac{\rho_{\text{nf}}}{\rho_{\text{bf}}}\right)^{0.8} \left(\frac{C_{p,\text{nf}}}{C_{p,\text{bf}}}\right)^{0.3} \left(\frac{\mu_{\text{bf}}}{\mu_{\text{nf}}}\right)^{0.5} \left(\frac{k_{\text{nf}}}{k_{\text{bf}}}\right)^{0.7} \tag{3.11}$$

A FOM parameter given for heat transfer with constant Reynolds number is given in equation (3.12) from [109]. This relation is commonly used in the literature [109].

$$FOM_{\text{Re}} = \left(\frac{h_{\text{nf}}}{h_{\text{bf}}}\right)_{\text{Re}} = \left(\frac{C_{p,\text{nf}}}{C_{p,\text{bf}}}\right)^{0.4} \left(\frac{\mu_{\text{nf}}}{\mu_{\text{bf}}}\right)^{0.4} \left(\frac{k_{\text{nf}}}{k_{\text{bf}}}\right)^{0.6} \tag{3.12}$$

A relation for the constant friction-related pumping power can be seen in equation (3.13) [109].

$$FOM_{pump} = \left(\frac{h_{\text{nf}}}{h_{\text{bf}}}\right)_r = \left(\frac{\rho_{\text{nf}}}{\rho_{\text{bf}}}\right)^{\frac{32}{55}} \left(\frac{C_{p,\text{nf}}}{C_{p,\text{bf}}}\right)^{\frac{2}{5}} \left(\frac{\mu_{\text{bf}}}{\mu_{\text{nf}}}\right)^{\frac{26}{55}} \left(\frac{k_{\text{nf}}}{k_{\text{bf}}}\right)^{\frac{3}{5}} \tag{3.13}$$

3.4.2 Statistics, approximations, and errors

discrepancy Δ, was calculated using equation (3.14). Where Δ_i is the value for each individual point. Superscript M is used to denote the model, whereas superscript E is used to denote experimentally derived values. The variable y represents the value being measured.

$$\Delta = \sum_{i=1}^{n} \Delta_i = \sum_{i=1}^{n} \frac{||y_i^M - y_i^E||}{y_i^E} \tag{3.14}$$

Linear interpolation between two points was done, using equation (3.15) from [24]. Where y is the desired vertical value that lies between the points denoted by subscript 1 and 0. x is the known horizontal value. Where y_1 and $x_1 > y_0$ and x_0.

$$y = \frac{(y_1 - y_0)(x - x_0)}{(x_1 - x_0)} + y_0 \tag{3.15}$$

The average, or mean was found by using equation (3.16). Where $\bar{a}$ is the average value and a_i is each individual value, to the number of measurements n.

$$\bar{a} = \frac{\sum_i^n a_i}{n} \tag{3.16}$$

The standard sample deviation*s* which provides a deviation from the desired value, has been found using equation (3.17) from [110]. Where s^2 is the variance. Due to the square, there are two possible values with a negative and positive sign.

$$s^2 = \frac{\sum_i^n (x_i - \bar{x})^2}{n-1} \tag{3.17}$$

The method of least squares, also known as linear regression from [110] is described in equation (3.18). Where x_i is the individual points along the x-axis, where $\bar{x}$ is the average x value. y_i represents the the individual values along the y-axis, where $\bar{y}$ is the average y value. The coefficient β represents the slope of the function, whereas the coefficient α represents the y-intercept point.

$$\beta = \frac{\sum_{i=1}^n (x_i - \bar{x})(y_i - \bar{y})}{\sum_{i=1}^n (x_i - \bar{x})^2}\ ,\ \alpha = \bar{y} - \beta\bar{x}$$

$$f(x) = \beta \cdot x + \alpha \tag{3.18}$$

Error and precision values for different important equipment and procedures used in this work are presented in table 3.5. All equipment was handled using the same operation procedure each time. Measurement error is either found in referenced documentation or calculated through standard deviation given in equation (3.17).

Table 3.5: Statistical and measurement error from important equipment and procedures

Type	Description	Measurement error	Precision	Comment
NDJ-8S	Viscometer	$\pm 3\%$ [100]	0.01mPa·s	–
UV-5100	Spectrophotometer	$\pm 0.5\%$ [111]	1 nm	–
Mastersizer 200	Dynamic light scatter	[96]	–	No error given in documentation
AG204	Scale	$\pm 0.069\%$ [112]	0.1 mg	–
THW-L2	Transient hot wire	$\pm 5\%$ [113]	$0.001 \mathrm{W/m \cdot K}$	
Dilutant	For spectral absorbency	± 0.659	–	Difference from 10 g of water
Sick ultrasonic flow meter	Flowmeter for internal flow	$\leq 2\ \%$ [114]	0.1 liter/min	–

Chapter 4

Results and Discussion

This chapter will present the results. The work that is presented is nanofluid stability, characterization of properties, optimal nanoparticle concentration for cooling, and engine testing. The chapter is also organized in this order.

4.1 Images from electron microscopy

The electron microscopy was carried out at the ELMI lab at the University of Bergen. Figure 4.1 shows images of four different particle agglomerates from dried-out samples. The aggregated sizes vary between small agglomerates $< 1\mu$m to agglomerates of many hundred micrometers. Figure 4.1a shows a linearly aggregated particle. Given the reference scale given at the bottom right in all images, it can be estimated that the aggregated particle is around 500-600 nm. The shape can be seen to consist of small almost spherical particles, which are carbon black. The aggregated particles in image 4.1b have formed a more lumped compact structure. Images 4.1c and 4.1d are of the same structure. The structure can be seen to be larger than the first two, with many smaller clusters surrounding it. Alterations in dried and dispersed cluster geometry are expected. Meaning that agglomerates would look different in a dried and dispersed state, due to all particle agglomerates being present on the same plane. Moreover, the images in figure 4.1 are different from the samples than the main ones studied in this work, with respect to particle concentration. This might additional differences in agglomeration.

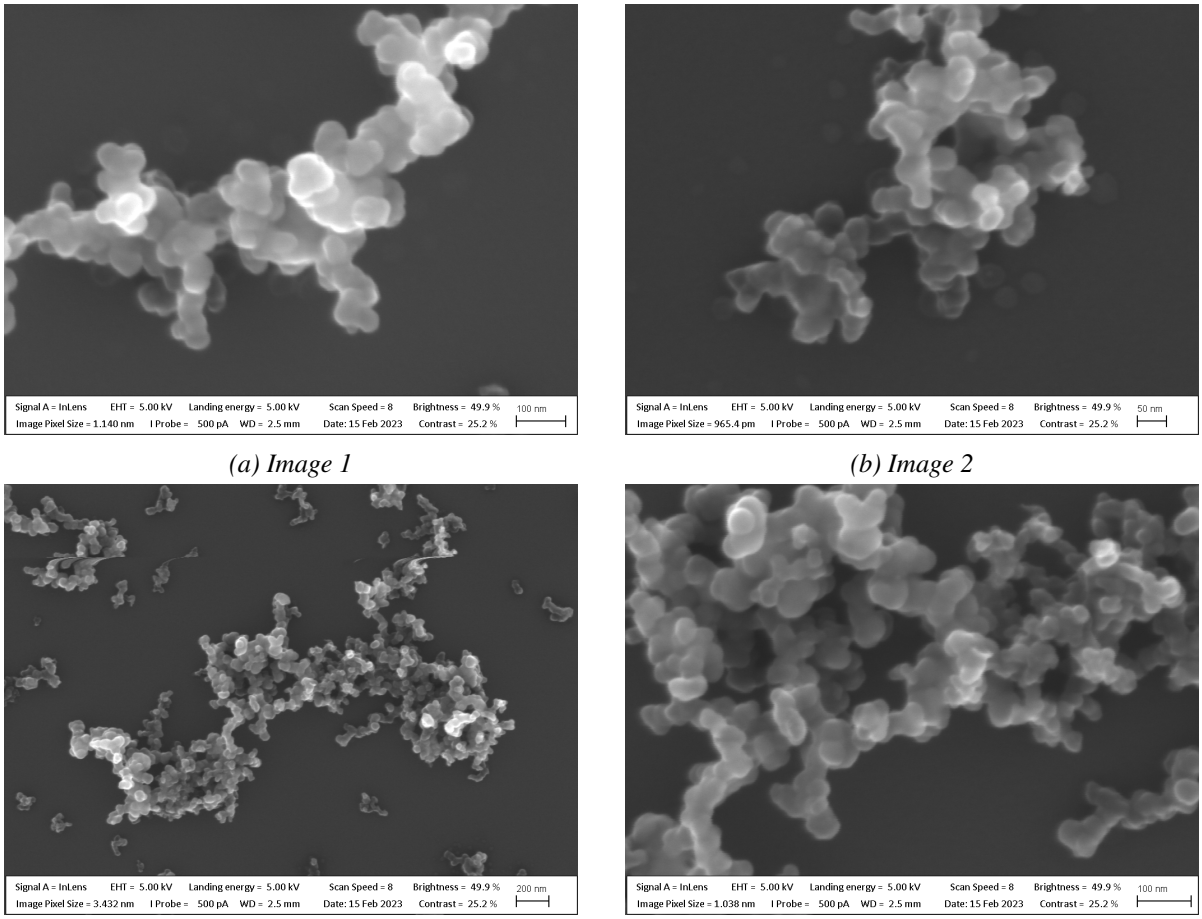

(a) Image 1 *(b) Image 2*

(c) Image 3 *(d) Image 4*

Figure 4.1: Electron microscopy of carbon black nanofluid sample. Images are taken at Bergen ELMI-LAB.

4.2 Particle size distribution of carbon black

Nanoparticle agglomeration sizes are crucial for determining nanoparticle stability. Smaller, more dispersed particles are ideal with regard to long-term stability. Higher temperatures in the fluids will increase the internal particle movement. This can potentially lead to higher agglomeration rates due to increased Brownian motion [28]. Because of this, it was expected both figure 4.4b and figure 4.2 which show results for cycled samples would show signs of larger particles.

Figure 4.2 shows the PSD for all six samples after every 10^{th} cycle. And figure 4.3 shows the PSD after one and two weeks. The accumulated aggregated particle volume in percent is shown along the y-axis and the average aggregated particle diameter along the x-axis in μm. Certain measurements from the PSD were classified as inaccurate, and have been purposefully left out of these figures. The affected measurements were for concentrations of 0.5wt.% for 0 cycles, 7.5wt.% for 30 cycles, 0.5wt.% for 1 week, and 1wt.% for 2 weeks. As is described in section 3.2.2, bubbles can be a source of measurement interference. All samples with the exception of 7.5wt.% for 30 cycles, exhibited the classical double peak behavior, with the second peak around 100μm. The sample of 7.5wt.% for 30 cycles was classified as one large peak between 100-700μm.

The previously discussed samples either inhibited characteristics of typical measurement interference (bubbles) or abnormally large agglomerates. The decision to leave them out was made, as they made it difficult to interpret the remaining data, whilst still shown in the figure. However, the software calculated average particle diameters presented in table 4.1 does contain these samples.

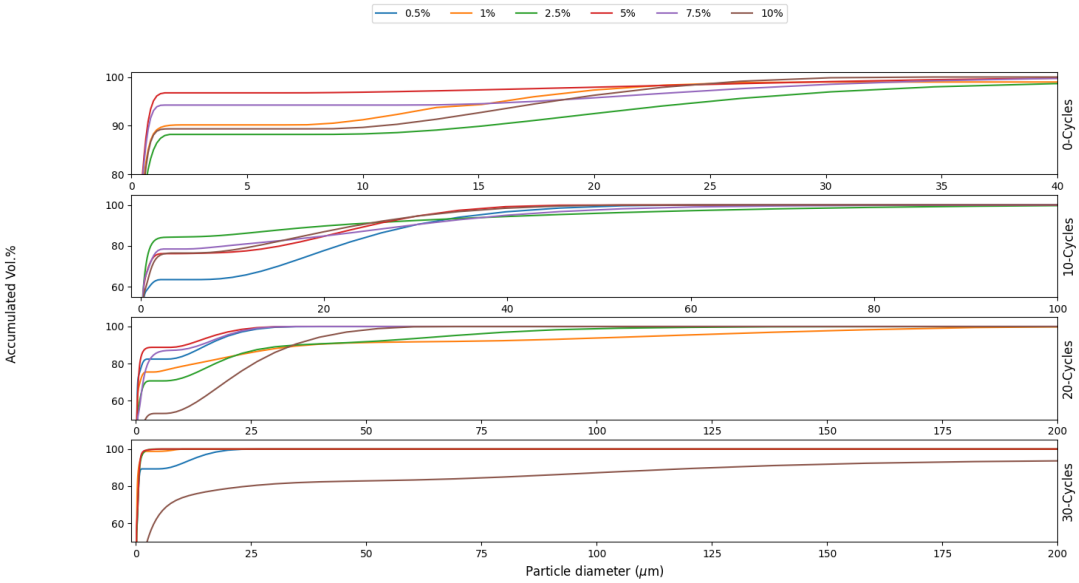

Figure 4.2: Particle size distribution of cycled samples

At zero cycles, between 85% and 95% of aggregated particles are close to or around 1 μm. Almost all particles are below 40 μm. It can be seen that the 5wt.% sample has the highest concentration of low-diameter particles. This is the case for 0, 20, and 30 cycles. For 0 cycles, it can be seen that 2.5wt.% have the highest concentrations of small aggregated particles.

At 30 cycles, 10wt.% is measured to contain much larger aggregated particles, than the rest of the samples in this cycle. Interestingly enough, the accumulated volume of cycles 10 and 20, generally have a higher concentration of larger-sized aggregated particles than 0 and 30 cycles. The general trend for cycles 10 and 20 is that there are higher fractions of larger aggregated particle sizes present. Whereas for 30 cycles, this upper bound of the aggregated particle sizes has increased substantially. Where about 90% of aggregated particles are measured to be below 200μm

Average aggregated particle diameters were calculated by the software from the average surface area for different cycled samples. The results can be seen in table 4.1. 0.5wt.% for 0 cycles and 7.5wt.% for 30 cycles can be seen here to be larger than the other samples. This is because of the distribution described earlier in this section. Most particle diameters can be seen to be in the magnitude of a few hundred nanometers. Where the smallest average sizes are below 100 nanometers. Furthermore, even with respect to thermal cycling, low average particle diameters can be seen. This indicates good dispersion for most of the fluids. For 0.5wt.% , an interesting trend is shown in the

data. It can be seen that the average particle diameter decreases with respect to the cycling. For all the other samples, a fluctuating average particle diameter can be observed.

When the nanofluids are subjected to repeated heating and cooling, natural convection will occur within the fluid. Higher temperatures will also generate more particle movement. A fluid containing more particles will also have a higher rate of particle-particle interactions. It is therefore expected that the general trend should indicate larger and larger agglomerates. However, even at 20 and 30 cycles, most particles, about 50-90% of particles are close to 0.2-1μm

When measuring the different samples, the particles were redistributed in the sample container through shaking. Larger agglomerates could have been sedimented by the samples that were measured. Meaning that the PSD would not be representative of the distribution of particles. Furthermore, large aggregated particles might have been stuck to the wall. The result of this seems to be that different samples include different variations of aggregated particle sizes.

Table 4.1: Average particle diameter in nm based on surface area

Cycle	0.5wt.% CB	1wt.% CB	2.5wt.% CB	5wt.% CB	7.5wt.% CB	10wt.% CB
0	263	106	104	90	89	98
10	186	657	124	152	164	182
20	147	163	188	119	194	289
30	99	102	97	93	945	321

Figure 4.3 shows the PSD of different nanofluid samples under static conditions. At one week it can be seen that both 5wt.% and 7.5wt.% have large concentrations of small particles. Which for the 5wt.% sample is around 96%. The remaining samples have a much lower concentration of fine particles. This trend continues for week two. At this point, there are formations of larger particles for all samples. This is the trend that was expected due to particle agglomeration from Brownian motion. The nanofluids were kept in stable conditions after the measurements were completed. By inspection, it could be seen that the nanofluids for all six particle concentrations were stable even 5 months after they were synthesized.

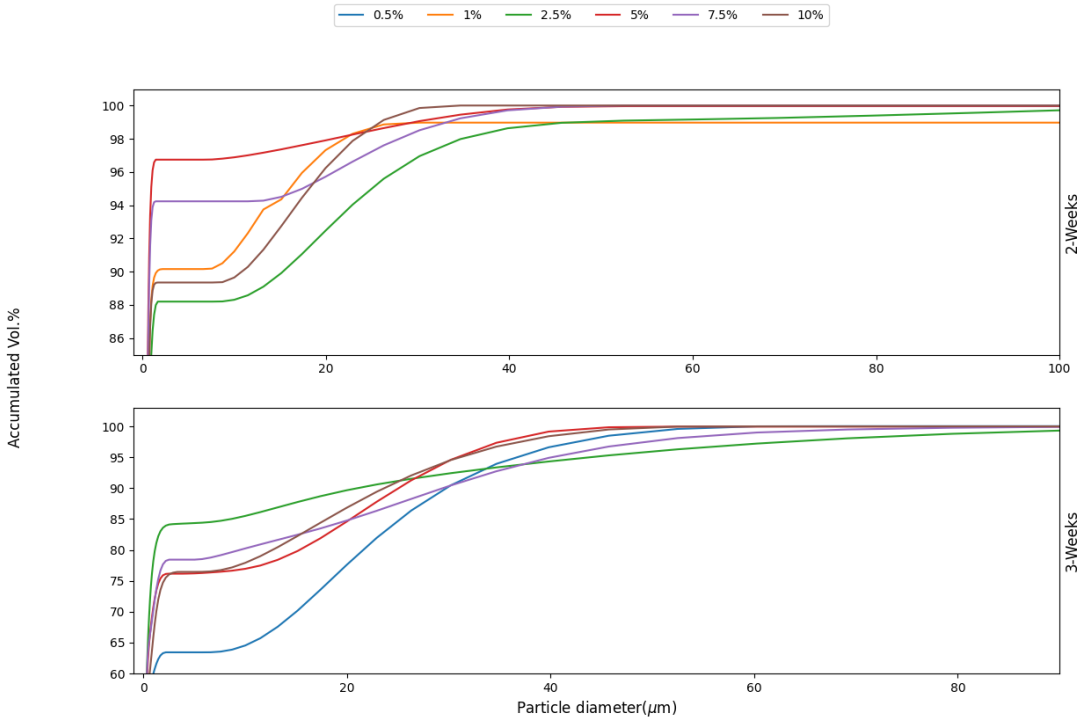

Figure 4.3: particle size distribution of static samples

4.3 Ultraviolet visible spectroscopy

UV visible spectroscopy was done to look at the local particle concentration density. Measurements were carried out with different samples under static and thermal load. The transmittance was calculated using the measured absorption coefficient with Beer-Lambert's equation given in (3.5).

The extinction coefficient values presented in figure 4.4 are the average values from wavelengths of 300-750nm. The vertical axis shows the average extinction in $\frac{1}{\mathrm{m}}$, whereas the horizontal axis shows the number of weeks under static load as in figure 4.4a. The horizontal axis in figure 4.4b shows the number of 10X cycles. It should also be noted that the extinction levels for 0.5wt.% is about three times greater, and about twice as great for 1wt.% compared to the actual samples. This is because the concentration of these samples had to be increased in the dilution process, to get measurements within the desired absorption range.

From figure 4.4a it can be seen that both the initial and final point lies around or below an extinction coefficient of 200. The only concentration above this point for the static samples is 10wt.% . However, there is little change from the 0 weeks samples to the 2-week-old samples.

When looking at cycled samples from figure 4.4b it can be seen that the four lowest concentrations have a much higher coefficient that the same points in figure 4.4a. The reason for this is unknown. It is however possible a slight variation in the added amount of particles during the dilution process could be the reason. During the measurements,

it was experienced that small variations in particle concentration had a large effect on the darkness intensity of the samples. The logic is, the darker the color, the more light would be absorbed, increasing the extinction coefficient.

At specific points, e.g. 10 and 20 cycles for 5wt.% . An increase in extinction levels can be seen. The cause of this might be the same as for the variation at the initial point, at zero cycles discussed above. In the figure, two grouping of points can be seen at 30 cycles. The top and bottom three concentrations all end up close to each other. The top three coefficients are around 400. This suggests that the 7.5wt.% and 10wt.% fluids could have sedimented more than the 5wt.% under the same cycled thermal load. This would be supported that higher temperatures can generate more particle aggregation [115], leading to quicker sedimentation. This is further supported by the fact that the higher-concentration sample's coefficients decline at a greater rate than the lower concentrations sample's coefficients. As an additional comment regarding the thermal cycling processes. Some researchers have registered foam formation to be a potential problem for certain surfactants under higher temperatures [3]. In this work, no notable foaming was experienced from the samples under thermal load.

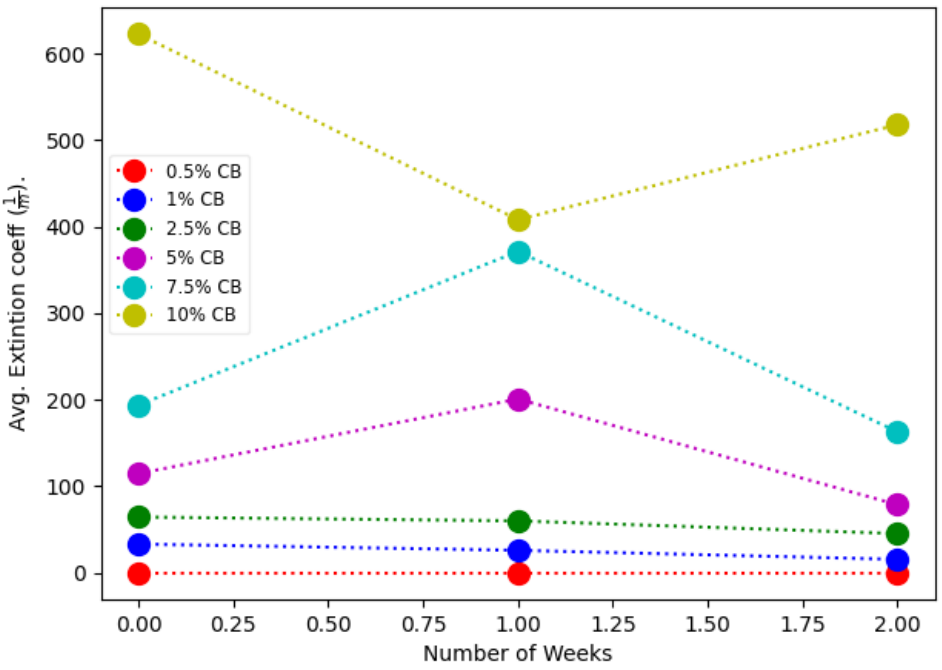

(a) Average extinction coefficient for samples under static load

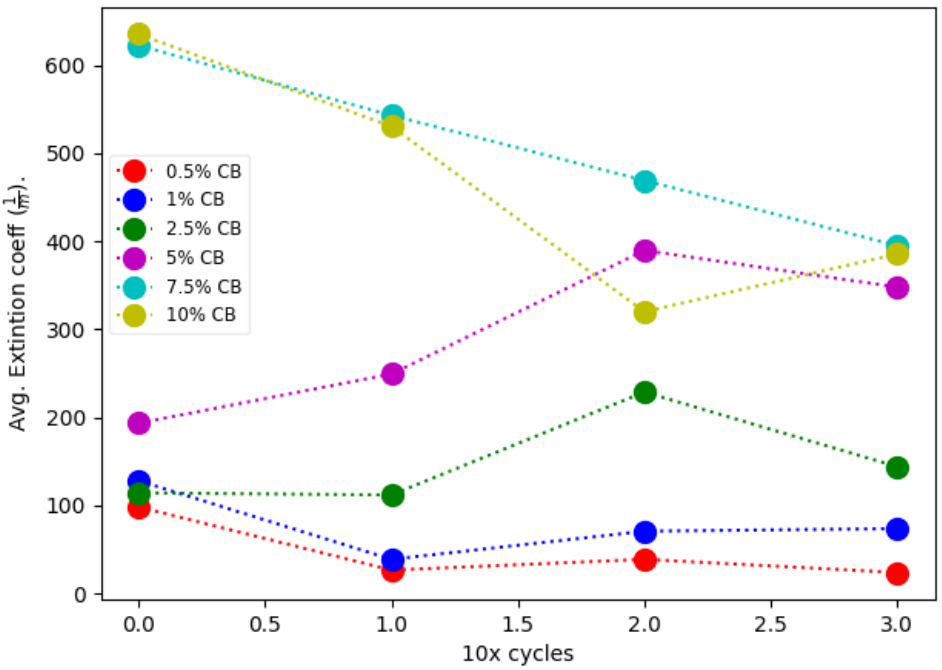

(b) Average extinction coefficient for samples under thermal load

Figure 4.4: Stability measurements of light transmittance

4.4 Characterization of viscosity

The tree sets referenced in table 3.3 are presented in this section. The measured viscosity of PVP diluted in water with respect to surfactant concentration can be seen in figure 4.5. There was measured an almost linear increase of viscosity with respect to PVP concentration in weight. The black vertical lines are the measurement deviation calculated with equation (3.17). A linear function was calculated using the method of least squares from equation (3.18) to approximate the trend of the viscosity increase. The line can be described as $f(x) = 2.7237 \cdot x + 0.2266$, where *f(x)* gives the viscosity in mPa·*s* and x is the surfactant concentration in percent weight. This would mean that the general trend for PVP in water is roughly an increase in 2.7 mPa·*s* per increase in percent weight. The increased viscosity is thought to be from the structure of the polymer. As the PVP molecules consist of long chains of molecules, it is thought possible that the long strains will cause internal entanglement when PVP binds to the water molecules. Increasing the molecular friction of the fluid.

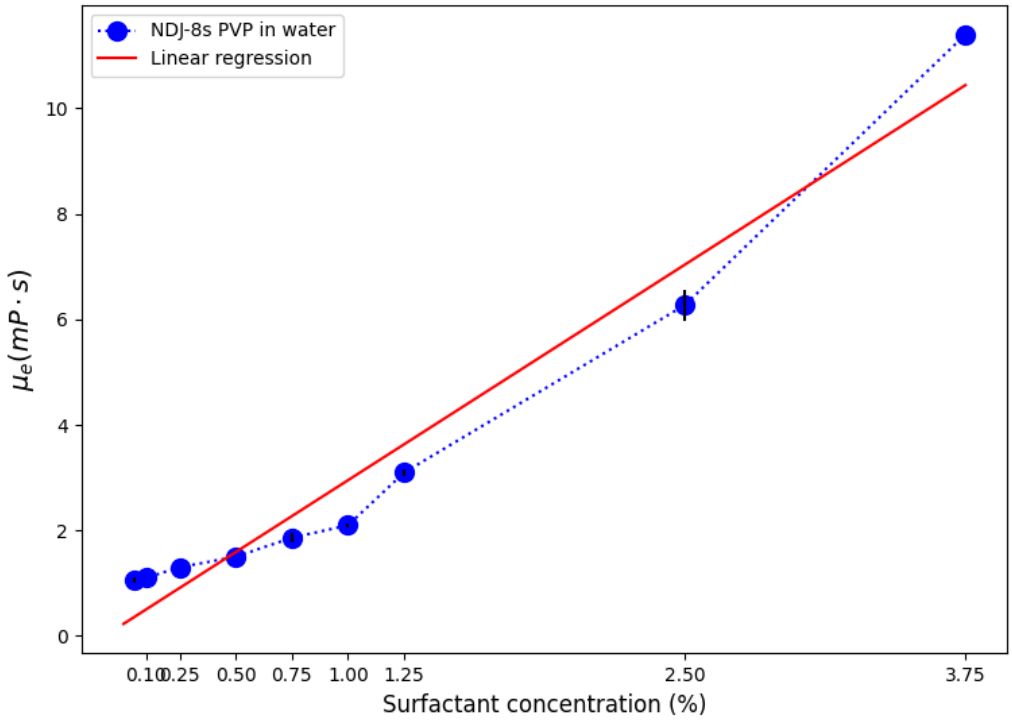

Figure 4.5: Viscosity measurements of different PVP concentrations diluted in water at 20°C

Figure 4.6 shows the change in viscosity with respect to particle concentration. For two different concentrations. These are set 1 and 2 as given in table 3.3. Points of set 2 (constant PVP) are measured with two different viscometers. These are given as relative in figure 4.6a with respect to the basefluids presented in figure 4.5 and as absolute in figure 4.6b. Figure 4.6a shows the relative increase from the basefluid. In this case, it would be relative to the PVP concentrations shown in figure 4.5. Contrary to what

would be expected, there the fluid viscosity is shown to increase non-linearly for both samples with constant and variable PVP levels. The two most interesting points are located at particle concentrations of 1 and 2.5wt.% . The measurements from the ball viscometer only had available at 35°C . This would mean that the viscosity would be slightly different from that measured at 20°C .

For the samples with variable PVP levels, it can be seen that there is an increase, until there is a sharp drop in viscosity levels at the point of 2.5wt.% particles, where the viscosity is at about 90% of water with 0.25wt.% PVP. From that point onwards, the viscosity increases steadily with the particle concentration. In the lines with constant PVP (0.5wt.%), a similar reduction is experienced at 1wt.% particles. In this case, the viscosity is close to 80% of the viscosity of PVP at 0.5wt.% In which PVP is at a 1:2 ratio to particles.

Figure 4.6b, shows how much PVP influences the viscosity. It can be seen that for the higher particle concentrations, there is a gap between the constant and variable PVP viscosity. With respect to absolute viscosity, it can be seen that the variable PVP viscosity is stable at around 1.2 mPa·s until a 2.5wt.% particle concentration. This is also the reason that the viscosity is higher at the lower particle concentrations for constant PVP levels, as the PVP concentration is much higher.

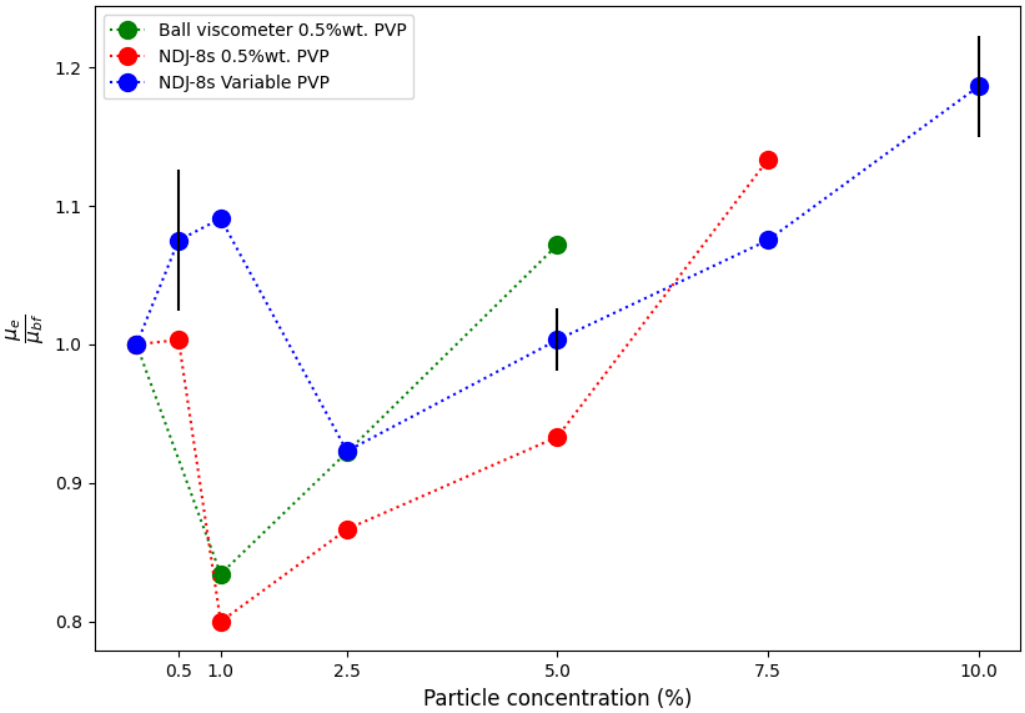

(a) Relative viscosity

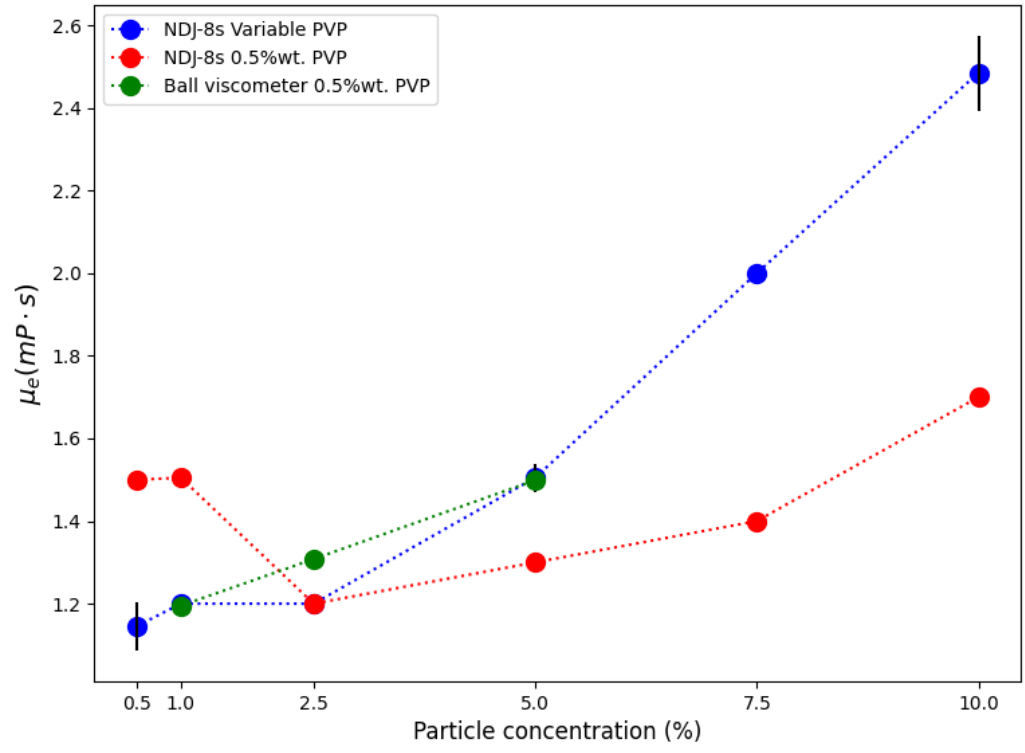

(b) Absolute viscosity

Figure 4.6: viscosity measurements at 20°C

Both Brinkmann's (2.3) and Einstein's (2.2) equations were compared to the variable PVP samples which are given in figure 4.7. Each equation is used twice to describe the increase in viscosity due to the added particle concentration. One variation uses a fixed viscosity, that of water. The second case uses the respective PVP viscosity for each data point. The calculated discrepancy for each function can be found in table 4.2. Both equations with respect to water can seem to differ greatly from the data points. When the respective viscosity of PVP at each point is used, it can be seen that the effects experienced from viscosity are indeed non-Einsteinan in nature. Both functions provide almost identical results with Brinkman's equation having a 0.01% less discrepancy from the data points. The real viscosity is less than the theoretical viscosity at the interval of 2.5wt.% to 7.5wt.% particle concentration. The highest viscosity discrepancy is for the point of 2.5wt.% which differs by almost 12% from what could be expected. Temperature as a possibility can be ruled out as the viscosity was measured at 20°C with the NDJ-8s viscometer.

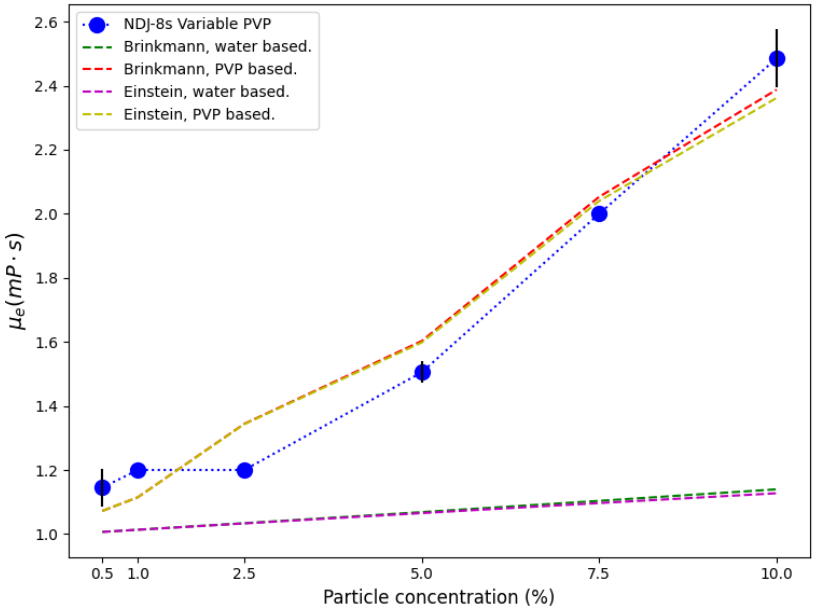

Figure 4.7: Viscosity models of Brinkman and Eistein to experimental data at 20 °C

Table 4.2: Discpreancy fractions for viscosity models

	Point						Total
	Δ_1	Δ_2	Δ_3	Δ_4	Δ_5	Δ_6	Δ
Brinkman PVP	0.063617	0.070985	0.120036	0.064889	0.026424	0.039239	0.064198
Brinkman water	0.120767	0.155441	0.138434	0.290074	0.448159	0.541403	0.282380
Einstein PVP	0.063646	0.071100	0.119189	0.061790	0.019959	0.049593	0.064213
Einstein water	0.120794	0.155546	0.139086	0.292140	0.451635	0.546345	0.284258

It was found that the addition of PVP greatly influences the nanofluid's viscosity. However, the addition of nanoparticles causes a Non-Einsteinian increase in fluid viscosity.

The cause of this phenomenon is unknown. Some authors have found similar effects for gold particles in PVP [66]. Some have described non-Einsteinian effects to be due to sonication [116], and some have pointed out a correlation between aggregated particle sizes and viscosity [53]. McElligot *et al.* [19] which studied ultra-low concentrations of functionalized graphene postulated that the viscosity will be reduced by the formation of a liquid layer at the hydrophobic part of the particles. At such surfaces, there is reduced friction between the water and the particle. This repulses water molecules, reducing the hydrogen bond strength. Carbon black is a hydrophobic particle. Gold can be hydrophobic given a contaminated surface [117]. the potential effects described by McElligot could be a viable theory. However, PVP increases the wettability of carbon black, helping it bind to water. This would mean that one end of the PVP molecule would bind to the particle and the other end would bind to the water molecules. This would cause hydrogen bonds at one end of the surfactant to reconnect and surround the hydrophobic particle. As the particles attach to the hydrophobic particle and water molecule it is expected that the viscosity would decrease again from when only PVP was dispersed in the liquid due to the formation of hydrogen bonds again.

4.5 Characterization of thermal conductivity

Thermal conductivity was first estimated using theoretical equations due to the unavailability of measurement equipment. Several models were tested before estimating thermal conductivity with Maxwell's equation. Other studies have also looked at Maxwell's equation as an estimation for thermal conductivity with varying success [40]. Figure 4.8 compares the Maxwell equation (2.10), Hamilton-Crosser (2.11), Wasp (2.12) and Pryazhnikov (3.6) to thermal conductivity data points from a previous thesis ([4]). The Thesis used the same carbon black particles as this thesis. The vertical axis shows absolute thermal conductivity for 20°C . The fractional discrepancy between the data points and in total for each model can be found in table 4.3. The discrepancy is calculated by equation (3.14).

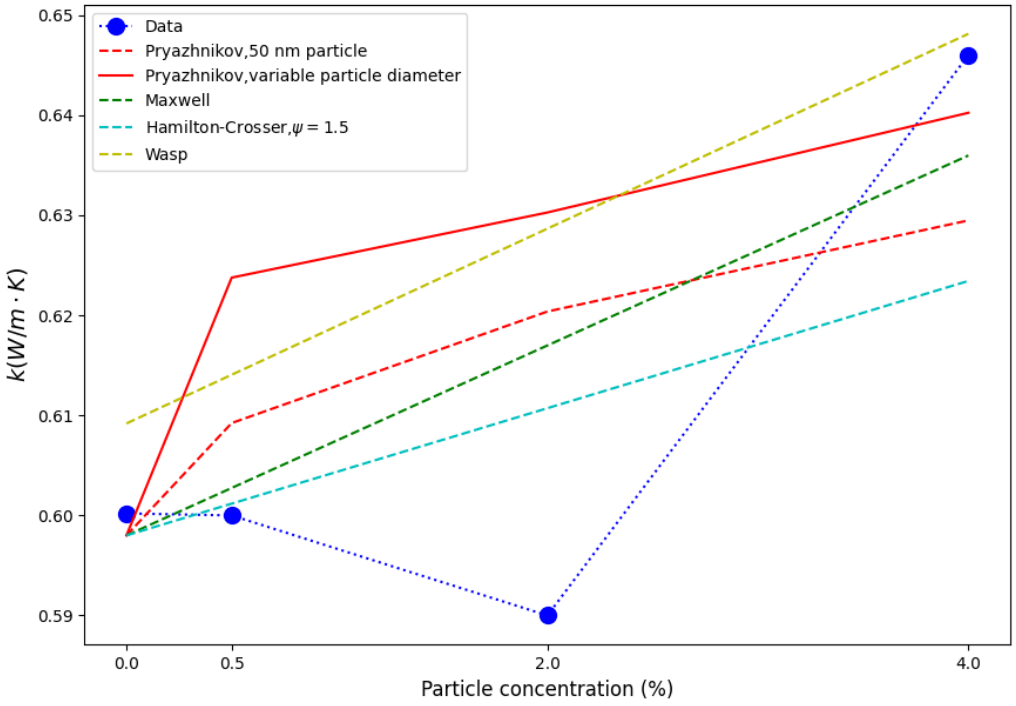

Figure 4.8: Theoretical models to measured thermal conductivity for 20°C from [4]

From the same figure, it can be seen that there is a variation in the trend for the four different data points. After the initial measurement, there is a slight reduction in thermal conductivity for 0.5wt.% particles, which is followed by another reduction for 2wt.% particles. For 4wt.% particles, there is an enhancement in thermal conductivity with about 8% from the thermal conductivity of water (0.598 W/mK). When regarding discrepancy point 4 in table 4.3, it can be seen that all models, with the exception of Hamilton-Crosser, are within 3% of the thermal conductivity at the final point. When regarding all points, Maxwell's equation is slightly better than Hamilton-Crosser's equation. The difference is that of 0.15%. As was described earlier in section 2.3.3. Maxwell's equation is the lower bound of the Hashin Shrikman inequality given

Table 4.3: Discrepancy fractions for different models of heat transfer

	Point				Total
	Δ_1	Δ_2	Δ_3	Δ_4	Δ
Pryazhnikov fixed	0.003665	0.015390	0.051488	0.025572	0.024029
Pryazhnikov variable	0.003665	0.039607	0.068261	0.008924	0.030114
Maxwell	0.003665	0.004579	0.045741	0.015528	0.017378
Hamilton-Crosser	0.003665	0.001966	0.035114	0.034935	0.01892
Wasp	0.014982	0.023431	0.065524	0.003295	0.026808

in (2.13). This means that Hamilton-Crosser's with a shape parameter of $\psi = 1.5$ will reduce the thermal conductivity outside of the lower bound for spherical particles ($\psi = 1$). This means that an imperfect particle will result in lower thermal conductivity. Two variations of Pryazhnikov have been used. One with a fixed particle diameter, and one with a variable aggregated particle diameter from table 4.1. The aggregated particle sizes that were used are estimates and are those for 0.5wt.% , 2.5wt.% , and 5wt.% at zero cycles.

Part of the work completed in this thesis has been to take measurements of thermal conductivity. The measured thermal conductivity of the reference value (de-ionized water) was measured to be 0.5584 $\mathrm{W/m \cdot K}$ at 20°C . The actual value is reported to be 0.598 $\mathrm{W/m \cdot K}$. The reference value is denoted by k_w. There are two figures that show the relative thermal conductivity with respect to the measured reference value, calculated by equation (3.4). One for the different PVP concentrations, provided in set 3 from table 3.3. And one where the thermal conductivity of the nanofluids is shown. Measurements were conducted at 21°C in both cases.

Figure 4.9 shows the relative increase in thermal conductivity of different concentrations of PVP diluted in water. Thermal conductivity can be seen to fluctuate with respect to the surfactant concentration. The upper bound is approximately 7% higher than water, whereas the lower bound is about the same as water.

The different equations that are used to predict thermal conductivity are Maxwell (2.10) and Pryazhnikov (3.6). Both equations use the same parameters as described in figure 4.8, with the exception of thermal conductivity for the basefluid. Where the thermal conductivity of the basefluid has been set to the measured value for water (0.5584 $\mathrm{W/m \cdot K}$).

In figure 4.10 two variations of Pryazhnikov's equation have been used. One with a fixed particle diameter of 50nm and one which takes into account the agglomerated particle sizes. The latter equation is an estimation of potential particle sizes. The particle sizes that were used are for zero cycles in table 4.1, with 0.5, 2.5, 7.5, and 10wt.% particles. It can be seen that a larger aggregated particle size corresponds to a larger rate of thermal conductivity. Maxwell, Hamilton-Crosser, and Wasp do not take particle size into consideration. The particle concentrations used in this thesis are larger than the ones used by Grebstad [4]. From the figure, it can be seen that for concentra-

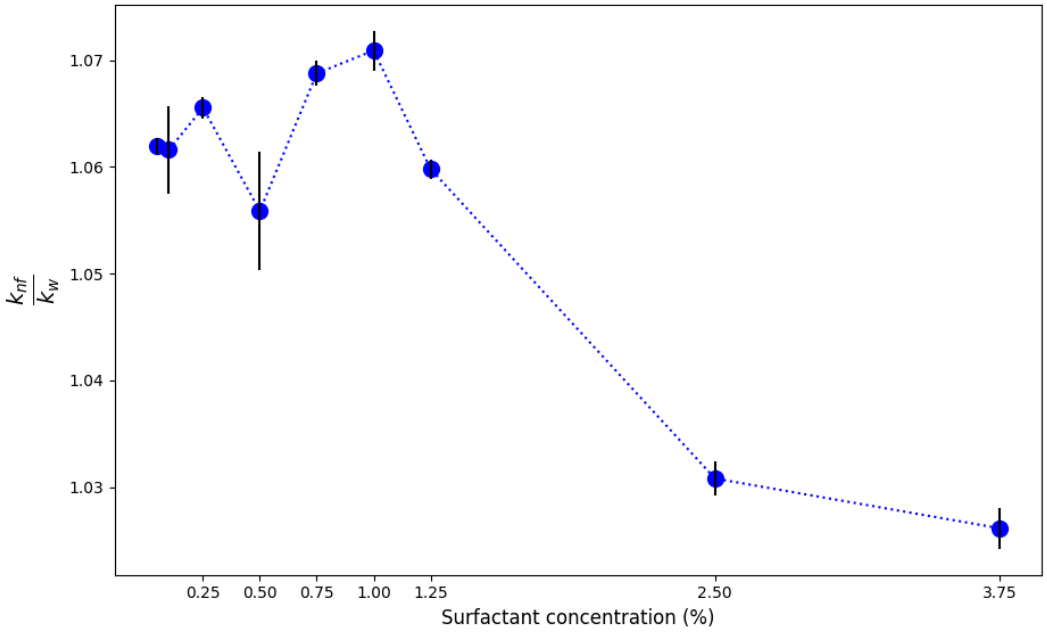

Figure 4.9: Measured thermal conductivity of different PVP concentrations diluted in water

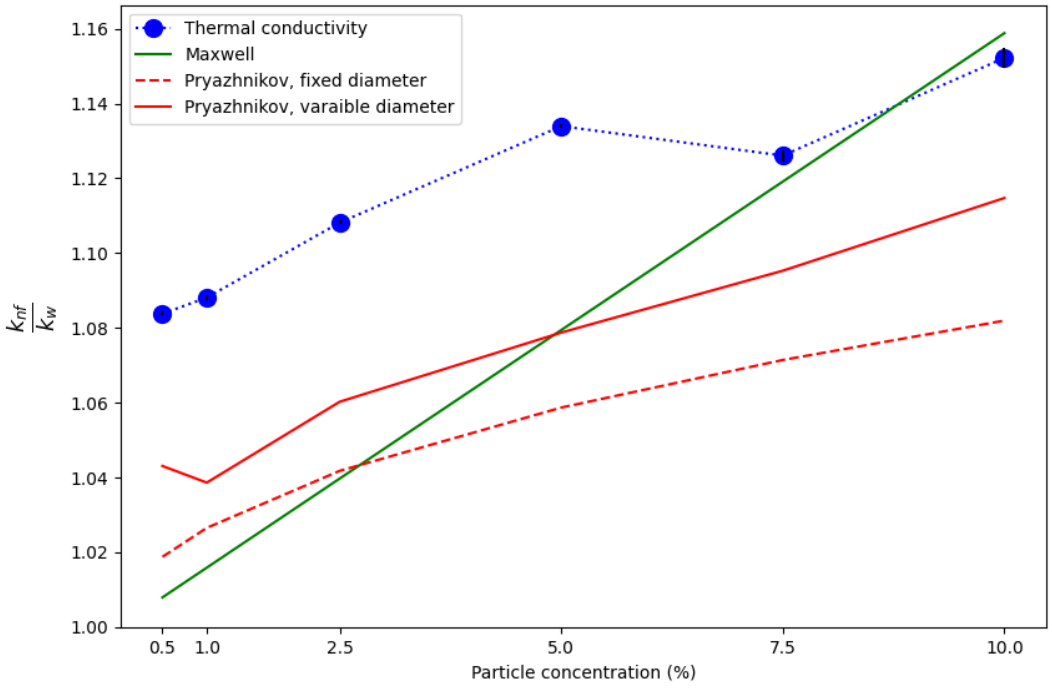

Figure 4.10: Measured thermal conductivity of nanofluids at 21°C compared to selected theoretical models

tions above 5wt.% , the predictions of thermal conductivity are greater using Maxwell's equation, than that of Pryazhnikov. Maxwell's equation is stated to be used as an estimate for low concentrations ($\varphi < 0.01$) of evenly distributed particles. A 5wt.% is equal to a volume fraction of $\varphi = 0.0261$ as can be seen in table 3.1. The measured thermal conductivity is noticeably higher than what was predicted by any of the models. At low concentrations, the thermal conductivity is enhanced between 8-13% compared to the measured value of water. At higher concentrations, Maxwell's equation is able to within reason predict the thermal conductivity of 7.5wt.% and 10wt.% nanofluids. It is possible that the enhancement at lower concentrations occurs due to a combination of the enhancement of the basefluid with the additional enhancement attributed by nanoparticles. The PVP would help increase the wettability of the nanoparticles, by binding one end to the water molecule and one end to the particle. It is possible that this structures the medium, and therefore increases thermal conductivity beyond what would be possible with particles only.

4.6 Figure of merit and engine testing

4.6.1 Figure of merit calculations

For the engine test, it was decided to study nanofluids with two different concentrations of carbon black. The two fluids used in this test were 0.5 and 2.5wt.% This decision was made with previous results for stability and the FOM relations, (3.9)-(3.13) shown in table 4.5. As different properties change with temperature e.g. thermal conductivity, it was deemed necessary to do the calculations using different temperatures. The temperatures are 20, 50, 70, and 90°C . Table 4.4 provides a list of the different thermophysical properties. The table shows the thermal conductivity using Maxwell's equation (2.10), as thermal conductivity was not measured at the time. Density is calculated using (3.1), heat capacity is calculated using (3.3), and viscosity is the experimental data from figure 4.7. All values were initially calculated (or measured) at 20°C . The basefluid of the nanofluid was assumed to have identical properties for thermal conductivity, heat capacity, and density to water, as these parameters were not known. Furthermore, it has been assumed the physical properties of the basefluid of the nanofluid scaled with the corresponding properties of water. Meaning that if water at 50°C has a 7% increase in thermal conductivity compared to water at 20°C , it is assumed that so does the basefluid of the nanofluid. This was done by finding the relative change with temperature of the desired property using equation (3.4).

The values from table 4.4 have been used to calculate FOMs for different temperatures in table 4.5. Here the nanofluids were compared to values of pure water. The equations that show an increased relative value are equations (3.9) and (3.12). The highest values from equation (3.9) can be found for 0.5wt.% and 2.5wt.% where the peak values in both cases can be located at 20°C , for which the maximum relative increase in net benefit is about 17%. The net bennefit decreases as the temperature increases. At 90 degrees for 2.5wt.% the net benefit is only 3.2% better. However, with the exception of FOM for constant Reynolds number all other FOMs point towards 0.5wt.% and

2.5wt.% to be the ideal concentrations.

Equation (3.12) is the FOM for constant Reynolds number (see equation (2.4)). This means that *Re* for the nanofluids are equal to that of the relative value, in this case water. The nanofluid and the relative fluid, here water have different densities and viscosities, see table 3.1 and 4.4. This means that the increase in fluid velocity must be equal to the relative difference in viscosity and density $\frac{\bar{\nu}_{\mathrm{nf}}}{\bar{\nu}_{\mathrm{bf}}} = \frac{\rho_{\mathrm{bf}}}{\rho_{\mathrm{nf}}} \frac{\mu_{\mathrm{nf}}}{\mu_{\mathrm{bf}}} \sim \frac{\mu_{\mathrm{nf}}}{\mu_{\mathrm{bf}}}$. The result of this effect would be that the nanofluid's velocity must be far greater than the relative fluid's velocity. With this in mind, it can be seen that the fluids with the higher particle concentration have a higher rate of heat transfer. However, to achieve an equal Reynolds number, the pump work would have to be increased significantly. This would cause the net benefit to disappear due to the increased pressure losses.

Table 4.4: Nanofluid properties for different temperatures

0.5wt.%	$T/(^{\circ}\mathrm{C})$	$k/(\frac{\mathrm{W}}{\mathrm{m}\cdot K})$	$\rho/(\frac{\mathrm{kg}}{\mathrm{m}^3})$	$C_\mathrm{p}/(\frac{\mathrm{kJ})}{\mathrm{kg}\cdot K}$	$\mu/(\mathrm{mPa}\cdot\mathrm{s})$
	20	0.6027	1000.5163	4.1826	1.1450
	50	0.6457	990.3735	4.1825	0.6247
	70	0.6649	980.1210	4.1823	0.4613
	90	0.6782	967.7043	4.182	0.3592
1.0wt.%	$T/(^{\circ}\mathrm{C})$	$k/(\frac{\mathrm{W}}{\mathrm{m}\cdot K})$	$\rho/(\frac{\mathrm{kg}}{\mathrm{m}^3})$	$C_\mathrm{p}/(\frac{\mathrm{kJ})}{\mathrm{kg}\cdot K}$	$\mu/(\mathrm{mPa}\cdot\mathrm{s})$
	20	0.6075	1002.8102	4.1654	1.2000
	50	0.6508	992.6945	4.1651	0.6548
	70	0.6701	982.4694	4.1647	0.4835
	90	0.6835	970.0858	4.1643	0.3764
2.5wt.%	$T/(^{\circ}\mathrm{C})$	$k/(\frac{\mathrm{W}}{\mathrm{m}\cdot K})$	$\rho/(\frac{\mathrm{kg}}{\mathrm{m}^3})$	$C_\mathrm{p}/(\frac{\mathrm{kJ})}{\mathrm{kg}\cdot K}$	$\mu/(\mathrm{mPa}\cdot\mathrm{s})$
	20	0.6217	1009.6192	4.1149	1.2000
	50	0.6660	999.5838	4.114	0.6548
	70	0.6858	989.4399	4.1131	0.4835
	90	0.6995	977.1547	4.1121	0.3764
5.0wt.%	$T/(^{\circ}\mathrm{C})$	$k/(\frac{\mathrm{W}}{\mathrm{m}\cdot K})$	$\rho/(\frac{\mathrm{kg}}{\mathrm{m}^3})$	$C_\mathrm{p}/(\frac{\mathrm{kJ})}{\mathrm{kg}\cdot K}$	$\mu/(\mathrm{mPa}\cdot\mathrm{s})$
	20	0.6455	1020.7302	4.0338	1.5050
	50	0.6914	1010.8259	4.0322	0.8212
	70	0.7120	1000.8146	4.0305	0.6063
	90	0.7262	988.6899	4.0284	0.4721
7.5wt.%	$T/(^{\circ}\mathrm{C})$	$k/(\frac{\mathrm{W}}{\mathrm{m}\cdot K})$	$\rho/(\frac{\mathrm{kg}}{\mathrm{m}^3})$	$C_\mathrm{p}/(\frac{\mathrm{kJ})}{\mathrm{kg}\cdot K}$	$\mu/(\mathrm{mPa}\cdot\mathrm{s})$
	20	0.6692	1031.5546	3.9565	2.0000
	50	0.7168	1021.7781	3.9542	1.0913
	70	0.7381	1011.8959	3.9518	0.8058
	90	0.7528	999.9276	3.9488	0.6273
10.0wt.%	$T/(^{\circ}\mathrm{C})$	$k/(\frac{\mathrm{W}}{\mathrm{m}\cdot K})$	$\rho/(\frac{\mathrm{kg}}{\mathrm{m}^3})$	$C_\mathrm{p}/(\frac{\mathrm{kJ})}{\mathrm{kg}\cdot K}$	$\mu/(\mathrm{mPa}\cdot\mathrm{s})$
	20	0.6929	1042.1033	3.8827	2.485
	50	0.7421	1032.4513	3.8798	1.3559
	70	0.7642	1022.6949	3.8767	1.0012
	90	0.7794	1010.8790	3.8729	0.7795

Table 4.5: Calculated FOM values for different particle concentrations

CB (wt.)	$T/(^{\circ}C)$	$FOM_{\text{V-D}}$ (3.9)	FOM_{Heat} (3.10)	FOM_{Cool} (3.11)	FOM_{Re} (3.12)	FOM_{Pump} (3.13)
0.50wt.%	20	1.172	0.9526	0.941	1.0582	0.9429
	50	1.0955	0.9526	0.9411	1.0582	0.9429
	70	1.0597	0.9526	0.9411	1.0582	0.9429
	90	1.0315	0.9526	0.9411	1.0582	0.9429
1.00wt.%	20	1.1599	0.9394	0.9248	1.0816	0.9263
	50	1.0842	0.9395	0.9249	1.0815	0.9263
	70	1.0488	0.9395	0.9249	1.0815	0.9263
	90	1.0209	0.9396	0.925	1.0815	0.9263
2.50wt.%	20	1.1726	0.9531	0.9416	1.0914	0.9383
	50	1.0961	0.9532	0.9417	1.0913	0.9384
	70	1.0604	0.9533	0.9418	1.0912	0.9384
	90	1.0322	0.9534	0.9420	1.091	0.9385
5.00wt.%	20	1.1149	0.8910	0.8655	1.2123	0.8608
	50	1.0423	0.8912	0.8657	1.2121	0.8609
	70	1.0084	0.8914	0.866	1.2119	0.861
	90	0.9818	0.8917	0.8662	1.2116	0.8611
7.50wt.%	20	1.0411	0.8132	0.7721	1.3774	0.7678
	50	0.9734	0.8134	0.7723	1.377	0.7679
	70	0.9418	0.8137	0.7726	1.3766	0.768
	90	0.917	0.814	0.773	1.3762	0.7682
10.00wt.%	20	0.9913	0.7618	0.7115	1.5226	0.7064
	50	0.9269	0.762	0.7118	1.522	0.7065
	70	0.8969	0.7624	0.7121	1.5215	0.7067
	90	0.8734	0.7628	0.7126	1.5208	0.7069

4.6.2 Rate of heat transfer from engine system

It was unknown how stable the fluids would be, due to orthokinetic sedimentation. An increased flow rate would accelerate this process. The tests however indicate good stability whilst flowing in complex geometry. During the tests, there was an issue with foam formation. Due to this, anti-foamer was added to the 2.5wt.% carbon black sample in a 1:1 ratio wt. with PVP.

Table 4.6 provides an overview of selected recorded data. Average values are calculated with equation (3.16). Standards deviation is calculated with equation (3.17). This has been done for the deviation from the expected flow and average temperature in and out of the engine.

Table 4.6: Selected measurements and deviation

Coolant	$\dot{V}_1$ /(liter/min)	$\bar{T}_\mathrm{i}$ /(°C)	$\bar{T}_\mathrm{o}$ /(°C)
EG+water	3 ±0.20	40.691±0.80	58.11 ±1.58
EG+water	4 ±0.10	43.625 ±0.31	56.41±0.23
EG+water	5 ±0.40	44.174 ±0.07	54.37±0.14
water	3 ±0.13	40.666±0.27	56.20 ±0.82
water	4 ±0.07	42.51 ±0.24	54.83 ±0.58
water	5 ±0.10	43.18 ±0.22	53.33 ±0.47
0.5%CB	3 ±0.09	40.46 0±0.49	55.76 ±0.57
0.5%CB	4 ±0.17	42.27 ±0.07	54.11 ±0.36
0.5%CB	5 ±0.16	43.11 ±0.14	52.54 ±0.27
2.5%CB	3 ±0.32	41.80 ±0.29	55.36 ±0.66
2.5%CB	4 ±0.23	43.41 ±0.17	54.71 ±0.53
2.5%CB	5 ±0.13	44.46 ±0.13	53.90 ±0.28

From the table, it can be seen that the inlet temperature is between 40 and 44 degrees. Whereas the outlet temperature is between 53 and 58°C . The general trend that can be seen is that all temperature differences decrease with an increased flow rate. The reference fluids have a higher temperature difference than the nanofluids at all flow rates. At a flow rate of 5 liters/ minute, the temperature difference between the reference coolants and the nanofluids is almost identical.

The rate of heat transfer was calculated using equation (3.7) using the described method from chapter 3. With the temperatures presented in table 4.6 The result of the calculations can be seen in figure 4.11. The figure shows two different calculations for heat transfer to the fluid. One with average volumetric flow 4.11a and one with the expected volumetric flow 4.11b. The expected heat transfer to the coolant is denoted by $\dot{Q}$ whereas the volumetric flow for the engine coolant is denoted by $\dot{V}_1$. The average volumetric flow is denoted by $\bar{\dot{V}}_1$.

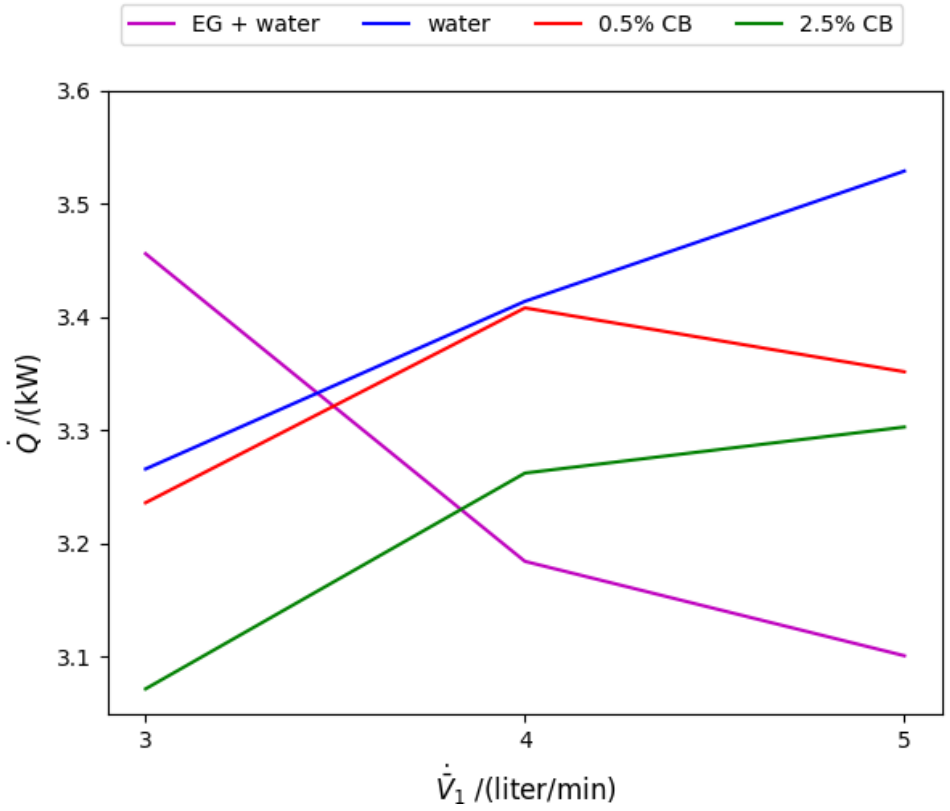

(a) Calculated heat transfer for coolants at different average volume flows

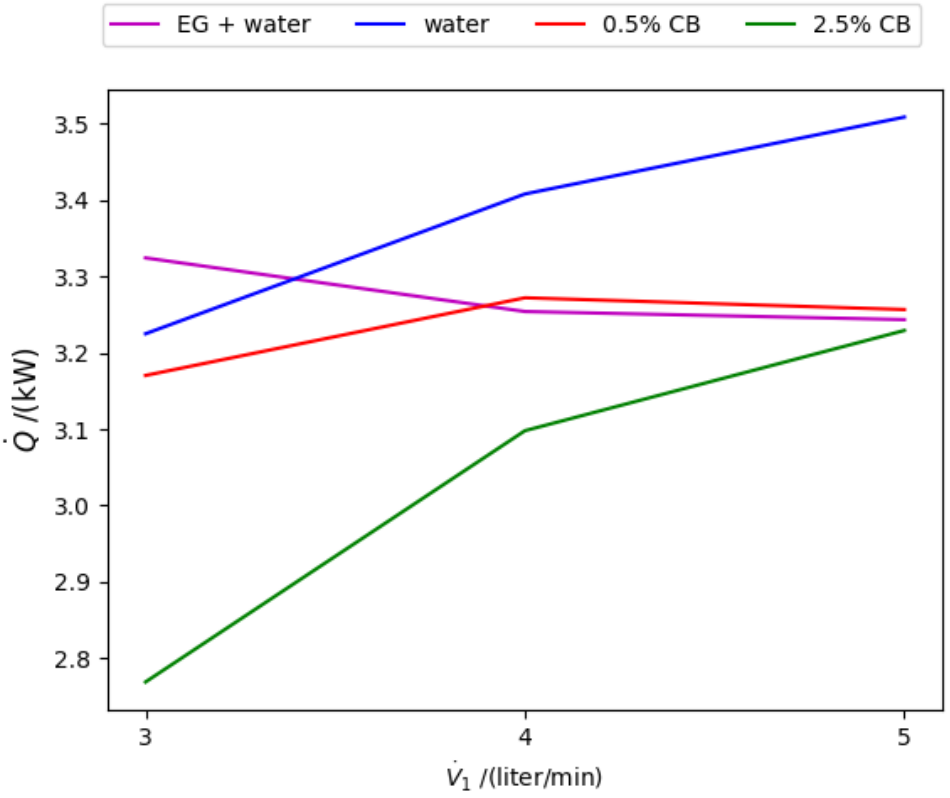

(b) Calculated heat transfer for coolants at different constant volume flows

Figure 4.11: Calculated heat transfer with average and constant volume flow

Bøthun [118] in his master's thesis estimated the heat transfer from the cylinder liner and cylinder head to the coolant of the Petter Diesel engine to be 3.42 kW. This estimate comes close to the calculated heat transfer presented in figure 4.11. The heat transfer in this case from the fluid can be seen to vary between approximately 2.8 kW to 3.55kW depending on the choice of volumetric flow. In figure 4.11a Water can be seen to have an almost linear increase in heat transfer with respect to the volumetric flow. This is the opposite of what can be seen for the EG and water mixture where the heat transfer decrease with volumetric flow. At 5 liters/ min, the 2.5% nanofluid can be seen to experience an increase in heat transfer whereas the 0.5% nanofluid decreases, and both fluids converge towards the same point.

At the flow rates provided, it can be seen that both the nanofluids have a higher heat rate than the EG mixture at flow rates of 4 and 5 liters/min. At 3 liters/min, EG, and water have the highest rate of heat transfer to the liquid. The fluid containing 2.5wt.% particles has an increased thermal conductivity and viscosity compared to the 0.5wt.% fluid. It is possible that the increased viscosity causes less convective heat transfer at lower volumetric flow rates. As the pump work is increased, a higher flow rate is obtained. It can be seen that the heat transfer to both water and the 2.5wt.% fluid increases. It is expected that the nanofluid coolants will require more pump work. Which would negate more of the potential upside of using them at higher flow rates.

Figure 4.11b shows a clearer picture of the correlation between the rate of heat transfer and flow rate. It is therefore suggested that small variations in the average flow rate from the dersired flow rate cause the non-linear cooling effects obtained in figure 4.11a.

In engine systems, convection is the dominant method of heat transfer. With the increase in flow rate, it is expected that the effects of forced convection are enhanced. As the fluid flow increases the Reynolds number would be increased with it. Where the flow would shift towards a more turbulent regime. This would cause more fluid would mix internally, which would decrease the thermal boundary layer and provide more liquid to the high-temperature components at lower temperatures. In situations where there would be a near-constant heat output, it can be expected that the temperature of the fluid would decrease with an increased flow rate. This is because the fluid is removed quicker from the area of contact with the fluid, meaning that less heat has the ability to be transferred from the area of contact to the fluid. It is however difficult to determine the effects of engine cooling. As the results obtained in this work lack a general trend. This could potentially have been found if more flow rates and fluids were tested. However, due to unexpected engine maintenance and delays, it was not possible to do all the desired tests within the given time frame of this work.

4.7 Summarizing discussion

From the UV-visible spectroscopy, a fluctuating particle concentration density for multiple nanofluid concentrations was recorded. The same varying trend from the number of recorded cycles could be seen for the PSD. However in general for 0, 10, 20, and

30 cycles, and 1 and 2 weeks. it seems like the majority of particles are in the low aggregated particle diameter range. Which indicates good dispersion of particles. Regarding the PSD of the cycled samples, the average aggregated particle diameter ranges increase, with respect to the number of cycles. An example is for 0 cycles where most samples are within 40μm, whereas for 10 cycles, most samples are within 100μm. However, with regard to the average aggregated nanoparticle diameter calculated from the surface area, no clear pattern is present. Moreover, a particle concentration of 5% seems to be ideal with respect to the particle concentration density in the UV visible spectroscopy and the stable particle size in the PSD. Some potential sources for fluctuating data points were discussed in sections 4.2 and 4.3. However, it would seem that PVP in the concentration range of 1:10 to particles is a good stabilizer for carbon black, even under thermal load.

Maxwell's equation was chosen for the FOM calculations before the thermal conductivity was measured. Maxwell was chosen based on comparison with available data and being the lower theoretical bound for thermal conductivity. From the actual measurements, it can be seen that Maxwell does not accurately depict the enhancement in thermal conductivity for lower-concentration nanofluids. However, at particle concentrations of 7.5 and 10wt.% Maxwell can be used. None of the other equations studied in this work can accurately depict thermal conductivity enhancement. The reason for this is unknown. However, as the thermal conductivity of the basefluid also saw a noticeable enhancement in thermal conductivity the base fluid could provide additional enhancement than the particles alone.

Most of the FOM calculations showed that nanofluids would not be an effective coolant compared to the values of water. However, these calculations were based on the thermal conductivity provided by Maxwell's equation, which has been found to not accurately describe most of the concentrations studied in this work. The output of equations is mostly dependent in this case on the viscosity and the thermal conductivity of the nanofluids. The addition of PVP and particles increases the viscosity but also the thermal conductivity. With the increased thermal conductivity it is expected that more equations would indicate increased benefit of using nanofluids compared to water.

It was not possible to classify whether the nanofluids are Newtonian, due to restrictions of the available shear rate of the NDJ-8s viscometer. As the influence of particles and surfactants has been shown to alter the physical properties of the basefluid, it could be that certain nanofluids studied in this work are non-Newtonian.

Different rheological classifications could also give more insight into how the rate of heat transfer would occur. All the different fluids that were tested as coolants exhibited different behavior at different flow rates. heat transfer to water linearly increased with the flow rate. Heat transfer to EG and water decreased with an increased flow rate. Nanofluid containing 0.5wt.% particles fluctuated with respect to the flow rate. Nanofluid containing 2.5wt.% particles had a non-linear increase in heat transfer with an increased flow rate. These variations are thought to stem from variations in the average flow.

4.8 Future Wok

The non-Einsteinian effects of viscosity experienced in this thesis should be investigated further by also seeing how the viscosity will change with temperature. Understanding this phenomenon could provide valuable information regarding the use of nanofluids in coolant applications. Direct use of this effect could be for the addition of more particles without greatly influencing the viscosity. Due to the time frame for the thesis, this phenomenon was not investigated further. However, as the viscosity of nanofluid coolants is of great interest there should be done more research in order to find a more ideal concentration of surfactants and particles to heat transfer. Additionally, there should be made an effort to investigate the rheological classification of the different nanofluids.

More tests with the engine at different flow rates are recommended as this can provide more data regarding heat transfer. As of today, the three points that are provided make it difficult to draw conclusions regarding the benefit of nanofluids as an engine coolant. Additionally, it could prove useful to obtain some data regarding the internal behavior of the nanofluid coolants. Like how much nucleate boiling occurs. Anti-foamer should also be considered for future tests. It would also be interesting to see how thermal cycling affects thermal conductivity. In order accurately determine the net benefit of nanofluids to other coolants, logging of the pump work should also be added as a data point as the nanofluids do have an increased viscosity.

Chapter 5

Conclusions

In order to determine whether nanofluids offer any benefits as a direct coolant in a CI engine four different objectives were formulated in 1.1. Carbon black nanoparticles have been shown to have good static and thermal stability when stabilized PVP (1:10 wt.) with sonication for 1 hour. Viscosity and thermal conductivity were studied theoretically and experimentally. It was found that the nanofluids had a non-Einsteinian increase in viscosity, which is theorized might be due to the properties of PVP. The increase in viscosity was not captured by Einstein's or Brinkman's equation. It has also been shown that the studied nanofluids with concentrations of 0.5-5% carbon black have an increased thermal conductivity which can not be described with classical effective medium theories or a more recent model. However, higher concentrations of 7.5 and 10% carbon black showed a correlation with Maxwell's equation. Nanofluids containing 0.5% and 2.5% carbon black were prepared for engine testing on the basis of FOM merit calculations. Where the majority of the equations showed that water was a more ideal coolant, using a thermal conductivity estimated by Maxwell's equation. From the engine testing, there was not found an easily described general trend as the nanofluid coolants have been found to behave differently at different flow rates. There is some indication that both nanofluids have a higher rate of heat transfer than the ethylene glycol and water mixture with a higher flow rate. Water has been found to have the highest heat transfer at 4 and 5 liters/min. Given that the rate of heat transfer for a flow rate of 4 liters/ minute with the 0.5% carbon black sample is almost identical. There is, therefore, some evidence that nanofluids could offer some benefit as a potential coolant, due to the increased thermal conductivity and relatively low viscosity increase associated with lower concentrations of carbon black and PVP. Additionally, the fluids have shown good stability. At this time, with the insights gained in this work, it is believed that the studied fluids would not offer any noticeable benefits as an engine coolant. More work is needed on the subject before a clear conclusion is drawn.

Appendix A

Raw data from CSV file

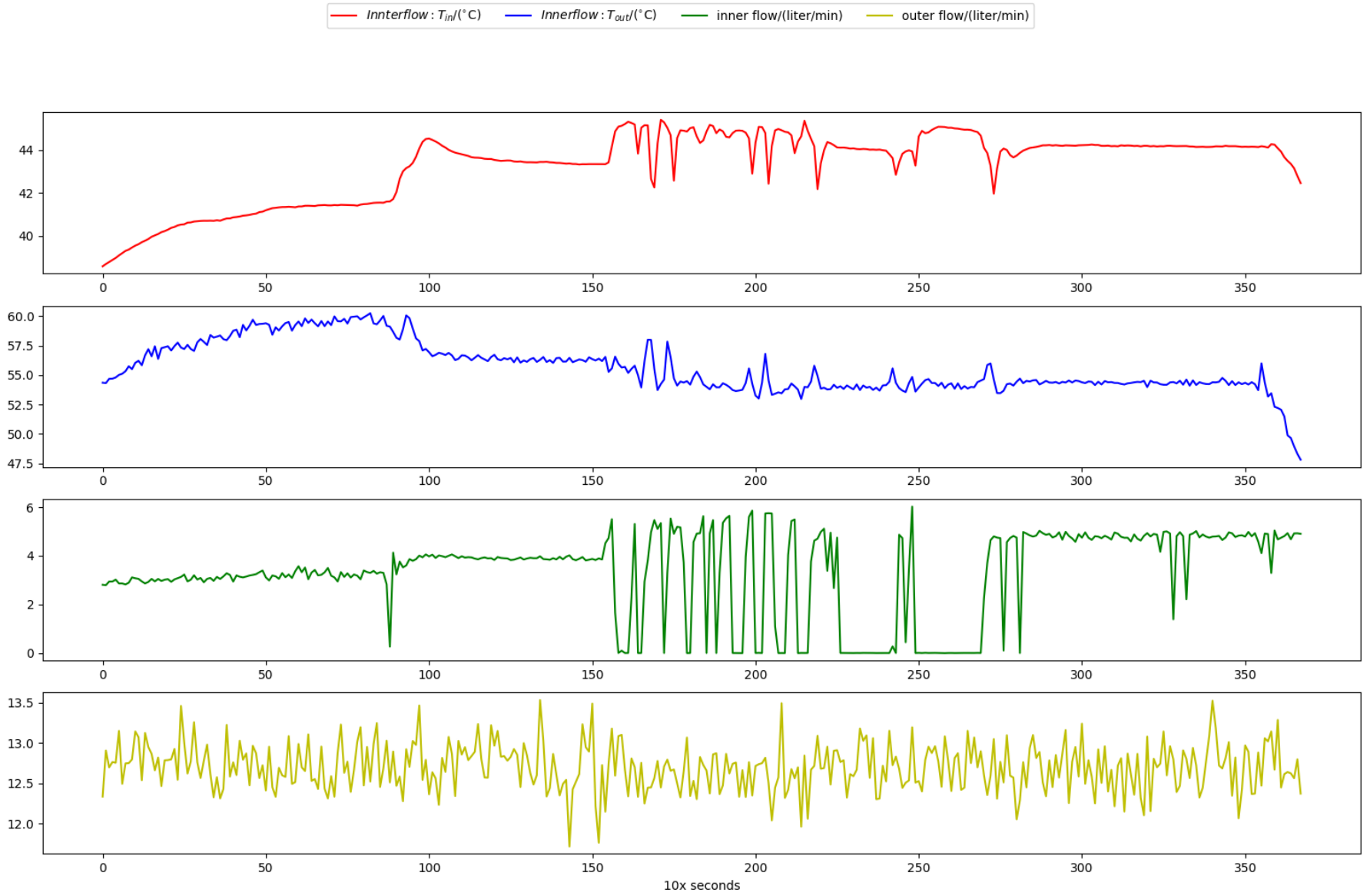

Figure A.1: Selected raw data of ethylene-glycol and water from CSV file

Bibliography

[1] W. L. McCabe, J. C. Smith, and P. Harriott, *Unit operations of chemical engineering*, vol. 7. McGraw-hill New York, 2005.

[2] A. R. I. Ali and B. Salam, "A review on nanofluid: preparation, stability, thermophysical properties, heat transfer characteristics and application," *SN Applied Sciences*, vol. 2, no. 10, pp. 1–17, 2020.

[3] S. Mukherjee, P. C. Mishra, and P. Chaudhuri, "Stability of heat transfer nanofluids–a review," *ChemBioEng Reviews*, vol. 5, no. 5, pp. 312–333, 2018.

[4] N. Grebstad, "Numerical investigation of the use of nanofluid in a photovoltaic thermal system," Master's thesis, The University of Bergen, 2022.

[5] E. Britannica, "Industrial revolution.." Web page. https://www.britannica.com/event/Industrial-Revolution. Accessed: 10/05/23.

[6] U. S. Dixit, M. Hazarika, J. P. Davim, U. S. Dixit, M. Hazarika, and J. P. Davim, "History of thermodynamics and heat transfer," *A Brief History of Mechanical Engineering*, pp. 73–97, 2017.

[7] S. U. Choi and J. A. Eastman, "Enhancing thermal conductivity of fluids with nanoparticles," tech. rep., Argonne National Lab.(ANL), Argonne, IL (United States), 1995.

[8] H. Masuda, A. Ebata, K. Teramae, and N. Hishinuma, "Alteration of thermal conductivity and viscosity of liquid by dispersing ultra-fine particles," *Netsu Bussei*, vol. 7, no. 4, pp. 227–233, 1993.

[9] W. Yu and H. Xie, "A review on nanofluids: preparation, stability mechanisms, and applications," *Journal of nanomaterials*, vol. 2012, 2012.

[10] E. Union, "setting co 2 emission performance standards for new heavy-duty vehicles and amending regulations (ec) no 595/2009 and (eu) 2018/956 of the european parliament and of the council and council directive 96/53/ec," 2019.

[11] B. Shadidi, G. Najafi, and T. Yusaf, "A review of hydrogen as a fuel in internal combustion engines," *Energies*, vol. 14, no. 19, p. 6209, 2021.

[12] C. D. Rakopoulos, D. C. Rakopoulos, G. M. Kosmadakis, and R. G. Papagiannakis, "Experimental comparative assessment of butanol or ethanol diesel-fuel

extenders impact on combustion features, cyclic irregularity, and regulated emissions balance in heavy-duty diesel engine," *Energy*, vol. 174, pp. 1145–1157, 2019.

[13] B. Ma, A. Yao, C. Yao, C. Chen, G. Qu, W. Wang, and Y. Ai, "Multiple combustion modes existing in the engine operating in diesel methanol dual fuel," *Energy*, vol. 234, p. 121285, 2021.

[14] J. R. Serrano, R. Novella, and P. Piqueras, "Why the development of internal combustion engines is still necessary to fight against global climate change from the perspective of transportation," 2019.

[15] W. Yu and S. Choi, "The role of interfacial layers in the enhanced thermal conductivity of nanofluids: a renovated maxwell model," *Journal of nanoparticle research*, vol. 5, pp. 167–171, 2003.

[16] K. V. Wong and O. De Leon, "Applications of nanofluids: current and future," *Advances in mechanical engineering*, vol. 2, p. 519659, 2010.

[17] S. E. Quiñones-Cisneros and U. K. Deiters, "Generalization of the friction theory for viscosity modeling," *The Journal of Physical Chemistry B*, vol. 110, no. 25, pp. 12820–12834, 2006.

[18] A. Einstein, *Eine neue bestimmung der moleküldimensionen*. PhD thesis, ETH Zurich, 1905.

[19] A. McElligott, A. Guerra, C. Y. Du, A. D. Rey, J.-L. Meunier, and P. Servio, "Dynamic viscosity of methane hydrate systems from non-einsteinian, plasma-functionalized carbon nanotube nanofluids," *Nanoscale*, vol. 14, no. 28, pp. 10211–10225, 2022.

[20] P. C. Mishra, S. Mukherjee, S. K. Nayak, and A. Panda, "A brief review on viscosity of nanofluids," *International nano letters*, vol. 4, pp. 109–120, 2014.

[21] J. P. Meyer, S. A. Adio, M. Sharifpur, and P. N. Nwosu, "The viscosity of nanofluids: a review of the theoretical, empirical, and numerical models," *Heat Transfer Engineering*, vol. 37, no. 5, pp. 387–421, 2016.

[22] H. C. Brinkman, "The viscosity of concentrated suspensions and solutions," *The Journal of chemical physics*, vol. 20, no. 4, pp. 571–571, 1952.

[23] R. L. Jaffe and W. Taylor, *The Physics of Energy*. Cambridge University Press, 2018.

[24] Y. Çengel, M. Boles, and M. Kanoglu, *Thermodynamics: An Engineering Approach*. McGraw-Hill series in mechanical engineering, McGraw-Hill Education, 2018.

[25] N. Lümmen, *Termodynamikk kort og godt*. Universitetsforlaget, 2020.

[26] W. A. Strauss, *Partial differential equations: An introduction*. John Wiley & Sons, 2007.

[27] J. McMurray and R. Fay, *Selected chapters from chemistry*. Pearson, 2012.

[28] S. M. Peker and S. S. Helvaci, *Solid-liquid two phase flow*. Elsevier, 2011.

[29] S. U. Ilyas, R. Pendyala, and N. Marneni, "Preparation, sedimentation, and agglomeration of nanofluids," *Chemical Engineering & Technology*, vol. 37, no. 12, pp. 2011–2021, 2014.

[30] Y. Ueki, T. Aoki, K. Ueda, and M. Shibahara, "Thermophysical properties of carbon-based material nanofluid," *International Journal of Heat and Mass Transfer*, vol. 113, pp. 1130–1134, 2017.

[31] Z. Said, A. Allagui, M. A. Abdelkareem, H. Alawadhi, and K. Elsaid, "Acid-functionalized carbon nanofibers for high stability, thermoelectrical and electrochemical properties of nanofluids," *Journal of colloid and interface science*, vol. 520, pp. 50–57, 2018.

[32] J. Wang, G. Li, T. Li, M. Zeng, and B. Sundén, "Effect of various surfactants on stability and thermophysical properties of nanofluids," *Journal of Thermal Analysis and Calorimetry*, vol. 143, pp. 4057–4070, 2021.

[33] A. Ghadimi, R. Saidur, and H. Metselaar, "A review of nanofluid stability properties and characterization in stationary conditions," *International journal of heat and mass transfer*, vol. 54, no. 17-18, pp. 4051–4068, 2011.

[34] E. E. Meyer, K. J. Rosenberg, and J. Israelachvili, "Recent progress in understanding hydrophobic interactions," *Proceedings of the National Academy of Sciences*, vol. 103, no. 43, pp. 15739–15746, 2006.

[35] M. Teodorescu and M. Bercea, "Poly (vinylpyrrolidone)–a versatile polymer for biomedical and beyond medical applications," *Polymer-Plastics Technology and Engineering*, vol. 54, no. 9, pp. 923–943, 2015.

[36] J. C. Maxwell, *A treatise on electricity and magnetism*, vol. 1. Clarendon press, 1873.

[37] J. Xu, B. Gao, and F. Kang, "A reconstruction of maxwell model for effective thermal conductivity of composite materials," *Applied Thermal Engineering*, vol. 102, pp. 972–979, 2016.

[38] I. Mugica and S. Poncet, "A critical review of the most popular mathematical models for nanofluid thermal conductivity," *Journal of Nanoparticle Research*, vol. 22, no. 5, p. 113, 2020.

[39] B. Tjaden, S. J. Cooper, D. J. Brett, D. Kramer, and P. R. Shearing, "On the origin and application of the bruggeman correlation for analysing transport phenomena in electrochemical systems," *Current opinion in chemical engineering*, vol. 12, pp. 44–51, 2016.

[40] J.-H. Lee, S.-H. Lee, C. Choi, S. Jang, and S. Choi, "A review of thermal conductivity data, mechanisms and models for nanofluids," *International journal of micro-nano scale transport*, 2011.

[41] T. Matsoukas and S. Lotfizadeh, "Colloidal thermal fluids," in *Encyclopedia of Surface and Colloid Science*, pp. 1–14, CRC Press, 2015.

[42] I. Gonçalves, R. Souza, G. Coutinho, J. Miranda, A. Moita, J. E. Pereira, A. Moreira, and R. Lima, "Thermal conductivity of nanofluids: a review on prediction models, controversies and challenges," *Applied Sciences*, vol. 11, no. 6, p. 2525, 2021.

[43] X.-Q. Wang and A. S. Mujumdar, "Heat transfer characteristics of nanofluids: a review," *International journal of thermal sciences*, vol. 46, no. 1, pp. 1–19, 2007.

[44] Z. Hashin and S. Shtrikman, "A variational approach to the theory of the effective magnetic permeability of multiphase materials," *Journal of applied Physics*, vol. 33, no. 10, pp. 3125–3131, 1962.

[45] R. S. Vajjha and D. K. Das, "A review and analysis on influence of temperature and concentration of nanofluids on thermophysical properties, heat transfer and pumping power," *International journal of heat and mass transfer*, vol. 55, no. 15-16, pp. 4063–4078, 2012.

[46] M. Chopkar, P. K. Das, and I. Manna, "Synthesis and characterization of nanofluid for advanced heat transfer applications," *Scripta Materialia*, vol. 55, no. 6, pp. 549–552, 2006.

[47] H. U. Kang, S. H. Kim, and J. M. Oh, "Estimation of thermal conductivity of nanofluid using experimental effective particle volume," *Experimental Heat Transfer*, vol. 19, no. 3, pp. 181–191, 2006.

[48] P. Keblinski, S. Phillpot, S. Choi, and J. Eastman, "Mechanisms of heat flow in suspensions of nano-sized particles (nanofluids)," *International journal of heat and mass transfer*, vol. 45, no. 4, pp. 855–863, 2002.

[49] A. Togo and I. Tanaka, "First principles phonon calculations in materials science," *Scripta Materialia*, vol. 108, pp. 1–5, 2015.

[50] R. Anufriev, A. Ramiere, J. Maire, and M. Nomura, "Heat guiding and focusing using ballistic phonon transport in phononic nanostructures," *Nature communications*, vol. 8, no. 1, p. 15505, 2017.

[51] S. P. Jang and S. U. Choi, "Role of brownian motion in the enhanced thermal conductivity of nanofluids," *Applied physics letters*, vol. 84, no. 21, pp. 4316–4318, 2004.

[52] P. Keblinski, R. Prasher, and J. Eapen, "Thermal conductance of nanofluids: is the controversy over?," *Journal of Nanoparticle research*, vol. 10, pp. 1089–1097, 2008.

[53] Y. He, Y. Jin, H. Chen, Y. Ding, D. Cang, and H. Lu, "Heat transfer and flow behaviour of aqueous suspensions of tio2 nanoparticles (nanofluids) flowing upward through a vertical pipe," *International journal of heat and mass transfer*, vol. 50, no. 11-12, pp. 2272–2281, 2007.

[54] J. Buongiorno, "Convective transport in nanofluids," 2006.

[55] D. Wen and Y. Ding, "Experimental investigation into convective heat transfer of nanofluids at the entrance region under laminar flow conditions," *International journal of heat and mass transfer*, vol. 47, no. 24, pp. 5181–5188, 2004.

[56] H. T. Klaus Mollenhauer, *Handbook of Diesel Engines*. Springer, 2009.

[57] J. B. Heywood, *Internal combustion engine fundamentals*. McGraw-Hill Education, 1988.

[58] M. Chandrasekar, S. Suresh, and T. Senthilkumar, "Mechanisms proposed through experimental investigations on thermophysical properties and forced convective heat transfer characteristics of various nanofluids–a review," *Renewable and Sustainable Energy Reviews*, vol. 16, no. 6, pp. 3917–3938, 2012.

[59] G. F. Smaisim, D. B. Mohammed, A. M. Abdulhadi, K. F. Uktamov, F. H. Alsultany, S. E. Izzat, M. J. Ansari, H. H. Kzar, M. E. Al-Gazally, and E. Kianfar, "Nanofluids: properties and applications," *Journal of Sol-Gel Science and Technology*, vol. 104, no. 1, pp. 1–35, 2022.

[60] A. Asadi, F. Pourfattah, I. M. Szilágyi, M. Afrand, G. Żyła, H. S. Ahn, S. Wongwises, H. M. Nguyen, A. Arabkoohsar, and O. Mahian, "Effect of sonication characteristics on stability, thermophysical properties, and heat transfer of nanofluids: A comprehensive review," *Ultrasonics sonochemistry*, vol. 58, p. 104701, 2019.

[61] Y.-H. Hung, T.-P. Teng, and B.-G. Lin, "Evaluation of the thermal performance of a heat pipe using alumina nanofluids," *Experimental Thermal and fluid science*, vol. 44, pp. 504–511, 2013.

[62] R. S. Khedkar, S. S. Sonawane, and K. L. Wasewar, "Heat transfer study on concentric tube heat exchanger using tio2–water based nanofluid," *International communications in Heat and Mass transfer*, vol. 57, pp. 163–169, 2014.

[63] M. C. S. Reddy and V. V. Rao, "Experimental investigation of heat transfer coefficient and friction factor of ethylene glycol water based tio2 nanofluid in double pipe heat exchanger with and without helical coil inserts," *International Communications in Heat and Mass Transfer*, vol. 50, pp. 68–76, 2014.

[64] N. Kannadasan, K. Ramanathan, and S. Suresh, "Comparison of heat transfer and pressure drop in horizontal and vertical helically coiled heat exchanger with cuo/water based nano fluids," *Experimental Thermal and Fluid Science*, vol. 42, pp. 64–70, 2012.

[65] J. A. Eastman, S. Choi, S. Li, W. Yu, and L. Thompson, "Anomalously increased effective thermal conductivities of ethylene glycol-based nanofluids containing copper nanoparticles," *Applied physics letters*, vol. 78, no. 6, pp. 718–720, 2001.

[66] A. Mishra, S. Ram, and G. Ghosh, "Dynamic light scattering and optical absorption in biological nanofluids of gold nanoparticles in poly (vinyl pyrrolidone) molecules," *The Journal of Physical Chemistry C*, vol. 113, no. 17, pp. 6976–6982, 2009.

[67] S. Choi, Z. G. Zhang, W. Yu, F. Lockwood, and E. Grulke, "Anomalous thermal conductivity enhancement in nanotube suspensions," *Applied physics letters*, vol. 79, no. 14, pp. 2252–2254, 2001.

[68] T. X. Phuoc, M. Massoudi, and R.-H. Chen, "Viscosity and thermal conductivity of nanofluids containing multi-walled carbon nanotubes stabilized by chitosan," *International Journal of Thermal Sciences*, vol. 50, no. 1, pp. 12–18, 2011.

[69] E. T. Ulset, P. Kosinski, and B. V. Balakin, "Solar steam in an aqueous carbon black nanofluid," *Applied Thermal Engineering*, vol. 137, pp. 62–65, 2018.

[70] D. Han, Z. Meng, D. Wu, C. Zhang, and H. Zhu, "Thermal properties of carbon black aqueous nanofluids for solar absorption," *Nanoscale research letters*, vol. 6, pp. 1–7, 2011.

[71] S. Hazra, S. Ghosh, and T. Nandi, "Photo-thermal conversion characteristics of carbon black-ethylene glycol nanofluids for applications in direct absorption solar collectors," *Applied Thermal Engineering*, vol. 163, p. 114402, 2019.

[72] Z. Meng, D. Han, D. Wu, H. Zhu, and Q. Li, "Thermal conductivities, rheological behaviors and photothermal properties of ethylene glycol-based nanofluids containing carbon black nanoparticles," *Procedia Engineering*, vol. 36, pp. 521–527, 2012.

[73] A. H. Shiravi, M. Shafiee, M. Firoozzadeh, H. Bostani, and M. Bozorgmehrian, "Experimental study on convective heat transfer and entropy generation of carbon black nanofluid turbulent flow in a helical coiled heat exchanger," *Journal of Thermal Analysis and Calorimetry*, vol. 145, pp. 597–607, 2021.

[74] K. Goudarzi and H. Jamali, "Heat transfer enhancement of al2o3-eg nanofluid in a car radiator with wire coil inserts," *Applied Thermal Engineering*, vol. 118, pp. 510–517, 2017.

[75] S. Sharma, "Fabricating an experimental setup to investigate the performance of an automobile car radiator by using aluminum/water nanofluid," *Journal of Thermal Analysis and Calorimetry*, vol. 133, no. 3, pp. 1387–1406, 2018.

[76] S. Peyghambarzadeh, S. Hashemabadi, M. S. Jamnani, and S. Hoseini, "Improving the cooling performance of automobile radiator with al2o3/water nanofluid," *Applied thermal engineering*, vol. 31, no. 10, pp. 1833–1838, 2011.

[77] S. Peyghambarzadeh, S. Hashemabadi, S. Hoseini, and M. S. Jamnani, "Experimental study of heat transfer enhancement using water/ethylene glycol based nanofluids as a new coolant for car radiators," *International communications in heat and mass transfer*, vol. 38, no. 9, pp. 1283–1290, 2011.

[78] K. Y. Leong, R. Saidur, S. Kazi, and A. Mamun, "Performance investigation of an automotive car radiator operated with nanofluid-based coolants (nanofluid as a coolant in a radiator)," *Applied Thermal Engineering*, vol. 30, no. 17-18, pp. 2685–2692, 2010.

[79] V. Delavari and S. H. Hashemabadi, "Cfd simulation of heat transfer enhancement of al2o3/water and al2o3/ethylene glycol nanofluids in a car radiator," *Applied thermal engineering*, vol. 73, no. 1, pp. 380–390, 2014.

[80] A. M. Hussein, H. Dawood, R. Bakara, and K. Kadirgamaa, "Numerical study on turbulent forced convective heat transfer using nanofluids tio2 in an automotive cooling system," *Case Studies in Thermal Engineering*, vol. 9, pp. 72–78, 2017.

[81] S.-C. Tzeng, C.-W. Lin, and K. Huang, "Heat transfer enhancement of nanofluids in rotary blade coupling of four-wheel-drive vehicles," *Acta Mechanica*, vol. 179, no. 1-2, pp. 11–23, 2005.

[82] A. M. Kumar, M. Kannan, and G. Nataraj, "A study on performance, emission and combustion characteristics of diesel engine powered by nano-emulsion of waste orange peel oil biodiesel," *Renewable Energy*, vol. 146, pp. 1781–1795, 2020.

[83] F. Micali, M. Milanese, G. Colangelo, and A. de Risi, "Experimental investigation on 4-strokes biodiesel engine cooling system based on nanofluid," *Renewable energy*, vol. 125, pp. 319–326, 2018.

[84] M. Muruganandam and P. M. Kumar, "Experimental analysis on internal combustion engine using mwcnt/water nanofluid as a coolant," *Materials Today: Proceedings*, vol. 21, pp. 248–252, 2020.

[85] L. M. Al-Harbi, S. A. Kosa, M. K. Baloch, Q. A. Bhatti, and E.-S. E.-B. H. El-Mossalamy, "Adsorption of polyvinylpyrrolidone over the silica surface: as affected by pretreatment of adsorbent and molar mass of polymer adsorbate," *International Journal of Polymer Science*, vol. 2016, 2016.

[86] Z. Mingzheng, X. Guodong, L. Jian, C. Lei, and Z. Lijun, "Analysis of factors influencing thermal conductivity and viscosity in different kinds of surfactant solutions," *Experimental Thermal and Fluid Science*, vol. 36, pp. 22–29, 2012.

[87] K. Pavithra, S. Gurumurthy, M. Yashoda, T. Mateti, K. Ramam, R. Nayak, and M. Murari, "Polymer-dispersant-stabilized ag nanofluids for heat transfer applications," *Journal of Thermal Analysis and Calorimetry*, vol. 146, pp. 601–610, 2021.

[88] S. Chakraborty and P. K. Panigrahi, "Stability of nanofluid: A review," *Applied Thermal Engineering*, vol. 174, p. 115259, 2020.

[89] K. Hong, T.-K. Hong, and H.-S. Yang, "Thermal conductivity of fe nanofluids depending on the cluster size of nanoparticles," *Applied Physics Letters*, vol. 88, no. 3, p. 031901, 2006.

[90] W. Yu, D. M. France, E. V. Timofeeva, D. Singh, and J. L. Routbort, "Comparative review of turbulent heat transfer of nanofluids," *International journal of heat and mass transfer*, vol. 55, no. 21-22, pp. 5380–5396, 2012.

[91] H. O'Hanley, J. Buongiorno, T. McKrell, and L.-w. Hu, "Measurement and model validation of nanofluid specific heat capacity with differential scanning calorimetry," *Advances in Mechanical Engineering*, vol. 4, p. 181079, 2012.

[92] S. Han, J. T. Lin, Y. Yamada, and D. Chung, "Enhancing the thermal conductivity and compressive modulus of carbon fiber polymer–matrix composites in the through-thickness direction by nanostructuring the interlaminar interface with carbon black," *Carbon*, vol. 46, no. 7, pp. 1060–1071, 2008.

[93] M. Kleiber1 and R. Joh, *VDI Heat atlas, D3.Liquids and Gases*. Springer, 2010.

[94] A. A. Balandin, "Thermal properties of graphene and nanostructured carbon materials," *Nature materials*, vol. 10, no. 8, pp. 569–581, 2011.

[95] M. R. Esfahani, E. M. Languri, and M. R. Nunna, "Effect of particle size and viscosity on thermal conductivity enhancement of graphene oxide nanofluid," *International Communications in Heat and Mass Transfer*, vol. 76, pp. 308–315, 2016.

[96] Malvern, "Mastersizer 200 user manual." Web page. https://www.malvernpanalytical.com/en/assets/Mastersizer-2000-user-manual-English-MAN0384-1-0_tcm50-11674.pdf Accessed: 09/05/23.

[97] Z. Xuan, Y. Zhai, M. Ma, Y. Li, and H. Wang, "Thermo-economic performance and sensitivity analysis of ternary hybrid nanofluids," *Journal of Molecular Liquids*, vol. 323, p. 114889, 2021.

[98] R. Sadeghi, S. G. Etemad, E. Keshavarzi, and M. Haghshenasfard, "Investigation of alumina nanofluid stability by uv–vis spectrum," *Microfluidics and Nanofluidics*, vol. 18, pp. 1023–1030, 2015.

[99] ELMILAB, "Instruments at elmilab." Web page. https://www.uib.no/en/elmi/154512/instruments Accessed: 03/04/23.

[100] "Ato-ndj series digital display viscometer instruction manual." WebPage. https://www.ato.com/Content/doc/ATO-NDJ-series-viscometer-instruction-manual.pdf Accessed: 08/04/23.

[101] R. Mostafizur, M. Rasul, and M. Nabi, "Effect of surfactant on stability, thermal conductivity, and viscosity of aluminium oxide–methanol nanofluids for heat transfer applications," *Thermal Science and Engineering Progress*, vol. 31, p. 101302, 2022.

[102] S. Lee, S.-S. Choi, S. Li, and J. Eastman, "Measuring thermal conductivity of fluids containing oxide nanoparticles," 1999.

[103] X. Zhang, H. Gu, and M. Fujii, "Effective thermal conductivity and thermal diffusivity of nanofluids containing spherical and cylindrical nanoparticles," *Experimental Thermal and Fluid Science*, vol. 31, no. 6, pp. 593–599, 2007.

[104] J. Eapen, R. Rusconi, R. Piazza, and S. Yip, "The classical nature of thermal conduction in nanofluids," 2010.

[105] M. Pryazhnikov, A. Minakov, V. Y. Rudyak, and D. Guzei, "Thermal conductivity measurements of nanofluids," *International Journal of Heat and Mass Transfer*, vol. 104, pp. 1275–1282, 2017.

[106] G. Paul, M. Chopkar, I. Manna, and P. Das, "Techniques for measuring the thermal conductivity of nanofluids: a review," *Renewable and Sustainable Energy Reviews*, vol. 14, no. 7, pp. 1913–1924, 2010.

[107] Numpy.org, "numpy.nan." Web page. https://numpy.org/doc/stable/reference/constants.html#numpy.nan Accessed: 30/05/23.

[108] I. Mouromtseff, "Water and forced-air cooling of vacuum tubes nonelectronic problems in electronic tubes," *Proceedings of the IRE*, vol. 30, no. 4, pp. 190–205, 1942.

[109] W. Yu, D. France, E. Timofeeva, D. Singh, and J. Routbort, "Thermophysical property-related comparison criteria for nanofluid heat transfer enhancement in turbulent flow," *Applied physics letters*, vol. 96, no. 21, p. 213109, 2010.

[110] G. Løvås, *Statistikk for universiteter og høgskoler*. Universitetsforlaget, 2013.

[111] Metash, "Uv-5100 uv/vis spectrophotometer users manual." User Manual.

[112] M. Toledo, "Ag204 operating instructions." Web page. https://www.mt.com/sg/en/home/library/operating-instructions/laboratory-weighing/AG.html Accessed: 09/05/23.

[113] T. instruments, "Transient hot-wire (thw-l2)." Web page. https://thermtest.com/thw-l2 Accessed: 23/05/23.

[114] SICK, "Sick nw20 ultrasonic flow sensor 60 litres / minute." Web page. https://www.axiscontrols.co.uk/products-services/products/sensors/liquid-flow-sensors/sick-nw20-ultrasonic-flow-sensor-60-litres-minute Accessed: 30/05/23.

[115] S. A. Adam, X. Ju, Z. Zhang, J. Lin, M. M. Abd El-Samie, and C. Xu, "Effect of temperature on the stability and optical properties of sio2-water nanofluids for hybrid photovoltaic/thermal applications," *Applied Thermal Engineering*, vol. 175, p. 115394, 2020.

[116] J.-H. Lee, K. S. Hwang, S. P. Jang, B. H. Lee, J. H. Kim, S. U. Choi, and C. J. Choi, "Effective viscosities and thermal conductivities of aqueous nanofluids containing low volume concentrations of al2o3 nanoparticles," *International Journal of Heat and Mass Transfer*, vol. 51, no. 11-12, pp. 2651–2656, 2008.

[117] T. Smith, "The hydrophilic nature of a clean gold surface," *Journal of Colloid and Interface Science*, vol. 75, no. 1, pp. 51–55, 1980.

[118] Lukas Brayn Bøthun, "Numerical simulation of nanofluid cooling in a single-cylinder diesel engine," 2023.